

PHASE EQUILIBRIA AND THERMODYNAMIC
STUDIES IN THE $\text{MnO}-\text{NiO}-\text{Cr}_2\text{O}_3$ SYSTEM
AT 1300°C

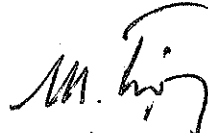
A MASTER THESIS
SUBMITTED TO THE DEPARTMENT OF METALLURGICAL ENGINEERING
AND THE COMMITTEE ON THE FACULTY OF ENGINEERING
OF MIDDLE EAST TECHNICAL UNIVERSITY
IN PARTIAL FULFILLMENT OF THE REQUIREMENTS
FOR THE DEGREE OF
MASTER OF SCIENCE

BY

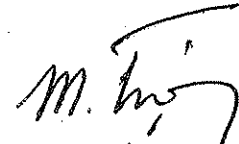
NURŞEN KOÇ

January 1981

I certify that I have read this thesis and that in my opinion it is fully adequate, in scope and quality, as a thesis for the degree of Master of Science.


Prof. Dr. Muharrem Timuçin
Supervisor

I certify that this thesis satisfies all the requirements as a thesis for the degree of Master of Science.


Prof. Dr. Muharrem Timuçin
Chairman of the Department

Examining Committee in Charge:

Associate Prof. Dr. Ahmet Seveci

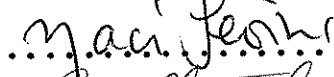
Ass. Prof. Dr. Maci Sevinç

Ass. Prof. Dr. Tugrul Miftioğlu


Ass. Prof. Dr. Yavuz Topkaya


Ass. Prof. Dr. Hüsnü Ermiş











Committee Chairman



ABSTRACT

PHASE EQUILIBRIA AND THERMODYNAMIC STUDIES
IN THE MnO - NiO - Cr₂O₃ SYSTEM AT 1300°C.

KOÇ NURŞEN

M.S. in Metallurgical Engineering

Supervisor: Prof.Dr. Muharrem Timuçin

January, 1981, 100 + XII page.

Equilibria between metallic nickel, a gas phase of known oxygen partial pressure and the solid solution phases in the MnO - NiO - Cr₂O₃ system at the temperature 1300°C have been determined by the quenching technique.

The stability field of chromite solution and direction of conjugation lines between the coexisting oxide and chromite solid solutions were determined.

The standard free energy of formation of the compound NiCr₂O₄ was measured as -17,484.8 ± 140 J/gfw, and that of MnCr₂O₄ was calculated as -41,588 J/gfw.

ÖZET

MnO-NiO-Cr₂O₃ SİSTEMİNİN 1300°C DE KATI HAL TERMO-DİNAMIĞI VE FAZ İLİŞKİLERİ ÜZERİNDE ÇALIŞMALAR

KOÇ NURŞEN

Met. Müh. Böl. Yüksek Lisans Tezi.

Tez Yöneticisi: Prof. Dr. Muharrem Timuçin
Şubat, 1981, 100 + XII sayfa.

1300°C de MnO-NiO-Cr₂O₃ sistemindeki metalik nikel, oksijen basıncı bilinen gaz fazı ve katı eriyikler arasındaki denge ani soğutma tekniği ile belirlenmiştir.

Kromit ve oksit eriyikleri arasındaki denk faz bağı çizgilerinin yönleri ile kromit eriyiklerinin kararlılık alanı belirlenmiştir.

NiCr₂O₄ bileşiğinin standard serbest oluşum enerjisi -17484.8 ± 140 J/gfağ olarak ölçülmüş ve MnCr₂O₄ bileşiğinin ki -41588 J/gfağ olarak hesaplanmıştır.

ACKNOWLEDGEMENTS

The author wishes to express her special thanks to Prof. Dr. Muharrem Timuçin for his guidance, supervision and suggestions throughout this study.

The author would also like to express her gratitude to the technical staff of the Metallurgical Engineering Department for their invaluable support till the completion of this thesis.

TABLE OF CONTENTS

ABSTRACT

ÖZET

ACKNOWLEDGEMENTS

TABLE OF CONTENTS

LIST OF FIGURE

LIST OF TABLES

NOMENCLATURE

	<u>PAGE</u>
CHAPTER I	
INTRODUCTION	1
CHAPTER II	
PREVIOUS WORK	
2.1. The Mn-O System	6
2.2. The Ni-O System	8
2.3. The MnO-NiO System	9
2.4. The Systems NiO-Cr ₂ O ₃ and MnO-Cr ₂ O ₃	11
CHAPTER III	
EXPRIMENTAL PROCEDURE	
3.1. Outline of the Experimental Procedure	15
3.2. Details	16
3.2.1. Starting Oxide Mixtures	16
3.2.2. Preparation of Oxide Mixtures	18
3.2.3. Equilibration Experiments	19

	<u>Page</u>
3. 2.3.1. Equilibration Furnace	19
3. 2.3.2. Gas Atmospheres	20
3.2.3.4. Sample Examination	25
 CHAPTER IV	
DATA and RESULTS	
4.1. The Ni-NiO Equilibrium	31
4.2. Activity-Composition Relations in MnO-NiO solid solutions.	33
4.3. Determination of the Nonstoichiometric Region of Nickel Chromite and Activities of NiO and Cr ₂ O ₃ in the Cr ₂ O ₃ -NiO System	38
4.4. The Stability of Manganese Chromite at 1300°C.	45
4.5. The Spinel + Oxide Phase Boundary	47
4.6. NiO Activities within the MnO-NiO-Cr ₂ O ₃ Ternary	47
4.6.1. NiO Activities in the Spinel + Cr ₂ O ₃ Field	47
4.6.2. NiO Activities in the Spinel Field	49
4.6.3. NiO Activities in the Spinel + Oxide Field	49
4.7. Other Thermodynamic calculations	58
4.7.1. Graphical Representation of NiO Activities	58
4.7.2. Activities of MnO and Cr ₂ O ₃ in the Spinel Field	60
4.7.3. Activities of MnO and Cr ₂ O ₃ in Manganese Chromite Solutions.	65
4.7.4. Standard Free Energy of Formation of MnCr ₂ O ₄	65
4.7.5. Activity-Composition Relations in MnCr ₂ O ₄ ⁻ NiCr ₂ O ₄ Solid Solutions	68
 CHAPTER V	
DISCUSSION and CONCLUSIONS	73
REFERENCES	81
APPENDIX I	84
APPENDIX II	89

LIST OF THE FIGURES

	<u>Page</u>
Figure 1. The solid solution series MnO - NiO and MnCr_2O_4 - NiCr_2O_4 in the MnO-NiO- Cr_2O_3 system.	2
Figure 2. The phase diagram for the system Mn-O between Mn and Mn_2O_3 compositions.	7
Figure 3. Activity - composition relations in MnO-NiO solid solutions.	10
Figure 4. The standard free energy of formation of $\text{NiO}\cdot\text{Cr}_2\text{O}_3$ from NiO and Cr_2O_3 .	14
Figure 5. Position of furnace, specimen and gas mixing system.	24
Figure 6. The flow rate calibration curve of CO capillary.	26
Figure 7. The flow rate calibration curve of H_2 capillary.	27
Figure 8. The flow rate calibration curve of CO_2 capillary.	28
Figure 9. The flow rate calibration curve of H_2 capillary.	29
Figure 10. Activity of NiO and MnO as a function of composition in the MnO-NiO system at 1300°C .	36
Figure 11. Activity of NiO and Cr_2O_3 as a function of composition in NiO- Cr_2O_3 join.	43

	<u>Page</u>
Figure 12. Stability field of spinel solid solutions at 1300°C. The numbers in brackets represent the samples selected for NiO activity determinations.	48
Figure 13. Changes in d-spacing with composition in the system MnO-NiO.	56
Figure 14. Activities of NiO in the system MnO-NiO-Cr ₂ O ₃ at 1300°C.	59
Figure 15. Ternary isotherm showing the constriction of (a). Positive tangent-intercepts, and (b). negative tangent-intercepts (T _{1,12}).	61
Figure 16. Activities of MnO, NiO, and Cr ₂ O ₃ in the system MnO-NiO-Cr ₂ O ₃ at the temperature 1300°C.	64
Figure 17. Activity-composition relations in the MnO-Cr ₂ O ₃ system.	67
Figure 18. NiO Activities along the join MnCr ₂ O ₄ - NiCr ₂ O ₄ .	69
Figure 19. Activities of NiCr ₂ O ₄ and MnCr ₂ O ₄ as a function of composition in the MnCr ₂ O ₄ -NiCr ₂ O ₄ system.	72
Figure 20. The micro-photograph of the sample containing clusters of nickel precipitates.	76
Figure 21. The micro-photograph of the sample containing uniform nickel precipitates.	77
Figure 22. log a _{NiO} versus $\frac{1}{T}$ diagram, which is obtained by using the previous ¹⁴ results.	85
Figure 23. $\Delta\bar{H}_{NiO}$ versus N _{NiO} diagram in NiO-MnO system.	86

LIST OF THE TABLES

	<u>Page</u>
Table I. Critical runs for the determination of the equilibrium $\text{NiO} = \text{Ni} + \frac{1}{2}\text{O}_2$ at 1300°C .	32
Table II. Activity measurements of NiO in the MnO - NiO system.	35
Table III. Activities of MnO in the MnO - NiO solid solutions.	39
Table IV. Activities of nickel oxide as a function of composition along the NiO - Cr_2O_3 join at 1300°C .	40
Table V. Activities of NiO and Cr_2O_3 in nickel chromite solutions.	42
Table VI. Phases present in the samples along the MnO - Cr_2O_3 join. ($T = 1300^\circ\text{C}$, $P_{\text{O}_2} = 10^{-8.18}$ atm)	46
Table VII. Data obtained in quenching experiments in the MnO - NiO - Cr_2O_3 system.	50
Table VIII. d_{200} as a function of composition in the MnO - NiO - Cr_2O_3 system, and activities of NiO and MnO.	57
Table IX. Activities of Cr_2O_3 in the MnO - Cr_2O_3 system at 1300°C .	66
Table X. Activities of NiCr_2O_4 and MnCr_2O_4 as a function of composition in the MnCr_2O_4 - NiCr_2O_4 .	71

Table XI. Log a_{NiO} as a function of composition in the MnO - NiO system at 900°, 1000° and 1200°C	87
Table XII. Activities of NiO as a function of composition at 1300°C.	88
Table XIII. Activity calculations of Cr_2O_3 in MnO - NiO - Cr_2O_3 system.	89
Table XIV. Activity calculations of MnO in the MnO - NiO - Cr_2O_3 system.	95

CHAPTER I
INTRODUCTION

The system $\text{MnO-NiO-Cr}_2\text{O}_3$ is a great deal of technological and scientific interest among metallurgists as well as ceramists and crystal chemists. This system is characterized at subsolidus temperatures by two distinct series of solid solutions as illustrated in Fig.1. At the base of the $\text{MnO-NiO-Cr}_2\text{O}_3$ composition triangle MnO and NiO , each with the simple cubic structure, form an unbroken series of solid solutions. Along the binaries $\text{MnO-Cr}_2\text{O}_3$ and $\text{NiO-Cr}_2\text{O}_3$ the chromite compounds $\text{MnO.Cr}_2\text{O}_3$ and $\text{NiO.Cr}_2\text{O}_3$ form, respectively. These compounds belong to the class of double oxides, having the formula XY_2O_4 , which crystallize with the same general structure as the mineral spinel $\text{Mg Al}_2\text{O}_4$.

The ideal spinel structure is cubic, and the smallest cell of the spinel lattice contains eight formula units, e.g. the elementary cell of the double oxide XY_2O_4 will be $[\text{XY}_2\text{O}_4]_8$. Hence the unit cell of spinel will contain 8X, 16Y, and 32 oxygen atoms. In the spinel structure, the relatively large O^{2-} anions form a f.c.c. lattice. Within this lattice there are 64 tetrahedral and 32 octahedral interstitial sites available to be occupied, respectively, by 8X and 16Y metal cations. Because of the large number of available interstitial sites the arrangement of the cations may vary

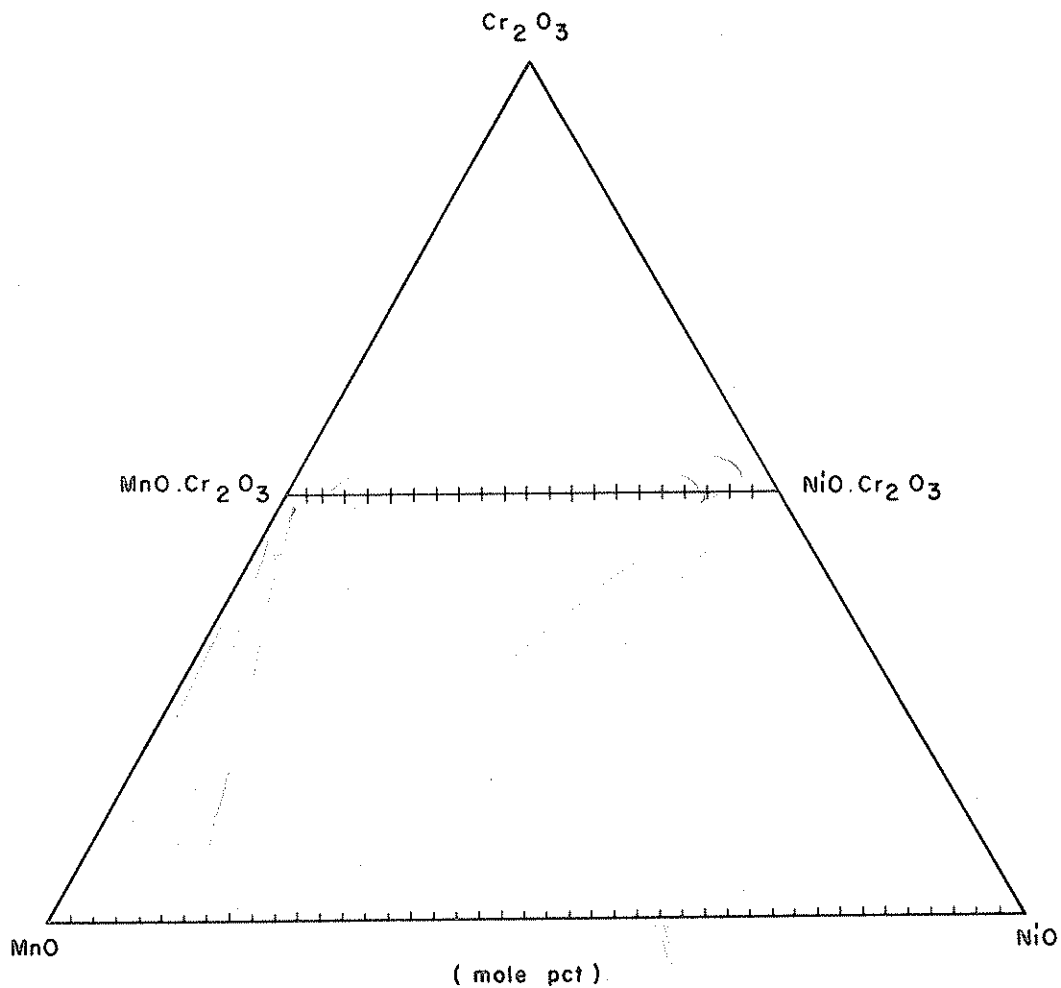


Figure 1 : The solid solution series $\text{MnO} - \text{NiO}$ and $\text{MnCr}_2\text{O}_4 - \text{NiCr}_2\text{O}_4$ in the $\text{MnO} - \text{NiO} - \text{Cr}_2\text{O}_3$ system.

considerably within certain limits. A "normal" double oxide spinel is defined as one in which all X ions occupy the tetrahedral and all Y ions occupy the octahedral sites. An "inverse" spinel has tetrahedral sites occupied by half of the Y ions, while the octahedral sites are occupied by X and remaining half of the Y ions. Between these two extreme cases intermediate distributions are also possible. The variations in distribution of cations in the X and Y positions cause marked changes in electrical and magnetic properties of the spinels. Hence the crystal chemists are interested in this aspect of spinel structure.

$\text{NiO} \cdot \text{Cr}_2\text{O}_3$ and $\text{MnO} \cdot \text{Cr}_2\text{O}_3$ are identified as normal spinels. These two compounds can form a continuous series of solid solutions as shown in Fig. 1. One particular field of application of transition metal spinel compounds in ceramics is their use in producing uniformly colored bodies. Both NiCr_2O_4 and MnCr_2O_4 , as well as their solid solutions, are useful for such applications.

In metallurgy, the system $\text{MnO} - \text{NiO} - \text{Cr}_2\text{O}_3$ comes into consideration in connection with the oxidation behavior of heat-resistance alloys. The nickel-chromium system has formed the basis for superalloys and heater materials for many years; hence, many studies have been

made on the oxidation of nickel base alloys. These studies revealed that in alloys having more than 30 wt pct Cr a protective layer of chromium sesquioxide (Cr_2O_3) forms which decreases the rate of oxidation.^{1,2} At lower chromium concentrations a complex scale of NiO, NiCr_2O_4 , and Cr_2O_3 forms which is also protective.² In order to protect steel and copper from oxidation in air at high temperatures, these materials are coated by Ni-Cr alloy,³ the protection is found to be due to the formation of a thick layer of NiCr_2O_4 . The addition of Mn to Ni-Cr alloys improves their oxidation resistance with the formation of an adherent, protective layer of MnCr_2O_4 .⁴ Lowell⁵ conducted one of the most comprehensive studies on the oxidation of Ni-Cr alloys; from X-ray diffraction and electron microprobe analyses of oxide layers formed at 1100°C and 1200°C he concluded that the source of improved protection of Ni-Cr-Mn alloys was the formation of adherent MnCr_2O_4 and $(\text{Mn},\text{Ni})\text{Cr}_2\text{O}_4$ layers. Hence the spinel solid solutions $(\text{MnO-NiO})\text{Cr}_2\text{O}_3$ are the products of oxidation of Ni-Cr-Mn alloys at elevated temperatures.

Although the kinetics of oxidation of Ni-Cr-Mn alloys appear to be well-studied, at least for commercial alloys, the thermodynamics of $(\text{Mn},\text{Ni})\text{Cr}_2\text{O}_4$ spinels are not examined at all. Consequently, the aim of the present thesis work was to obtain activity and phase equilibrium data in the system $\text{MnO-NiO-Cr}_2\text{O}_3$ with particular attention

to the spinel solid solutions. The specific objects of the present work, at the experimental temperature of 1300°C, were:

1. To determine the stability of the NiCr_2O_4 compound,
2. To determine the activities of NiO in solid solution phases and in some two-phase regions of the $\text{MnO-NiO-Cr}_2\text{O}_3$ system,
3. To determine the compositions of conjugate oxide and spinel solutions, and
4. To derive information on the stability of the MnCr_2O_4 compound and activity-composition relations in $\text{NiCr}_2\text{O}_4\text{-MnCr}_2\text{O}_4$ solid solutions.

CHAPTER II

PREVIOUS WORK

A complete thermodynamic study covering all the phases present in the system MnO- NiO- Cr₂O₃ is not available in the previous literature. However, portions of the system are examined in some detail. The information gathered in earlier investigations are presented in the following.

2.1 The Mn-O System

Phillips and Muan⁶ determined the phase relations in the system Mn-O as a function of temperature and oxygen partial pressure, within the composition interval Mn-Mn₂O₃. The phase diagram resulting from their work is shown in Fig.2. The solid lines of the diagram are phase boundaries and the dashed lines represent the oxygen partial pressures in equilibrium with the condensed phases. According to this diagram, MnO is a non-stoichiometric compound, with considerable excess of oxygen over the stoichiometric formula, particularly at temperatures above 1000°C. At 1300°C, for example, it is possible to prepare MnO of compositions ranging from point (a) to point (b) by manipulating the oxygen partial pressures of the gas phase. MnO at point (b) is perfectly stoichiometric, and the partial pressure of

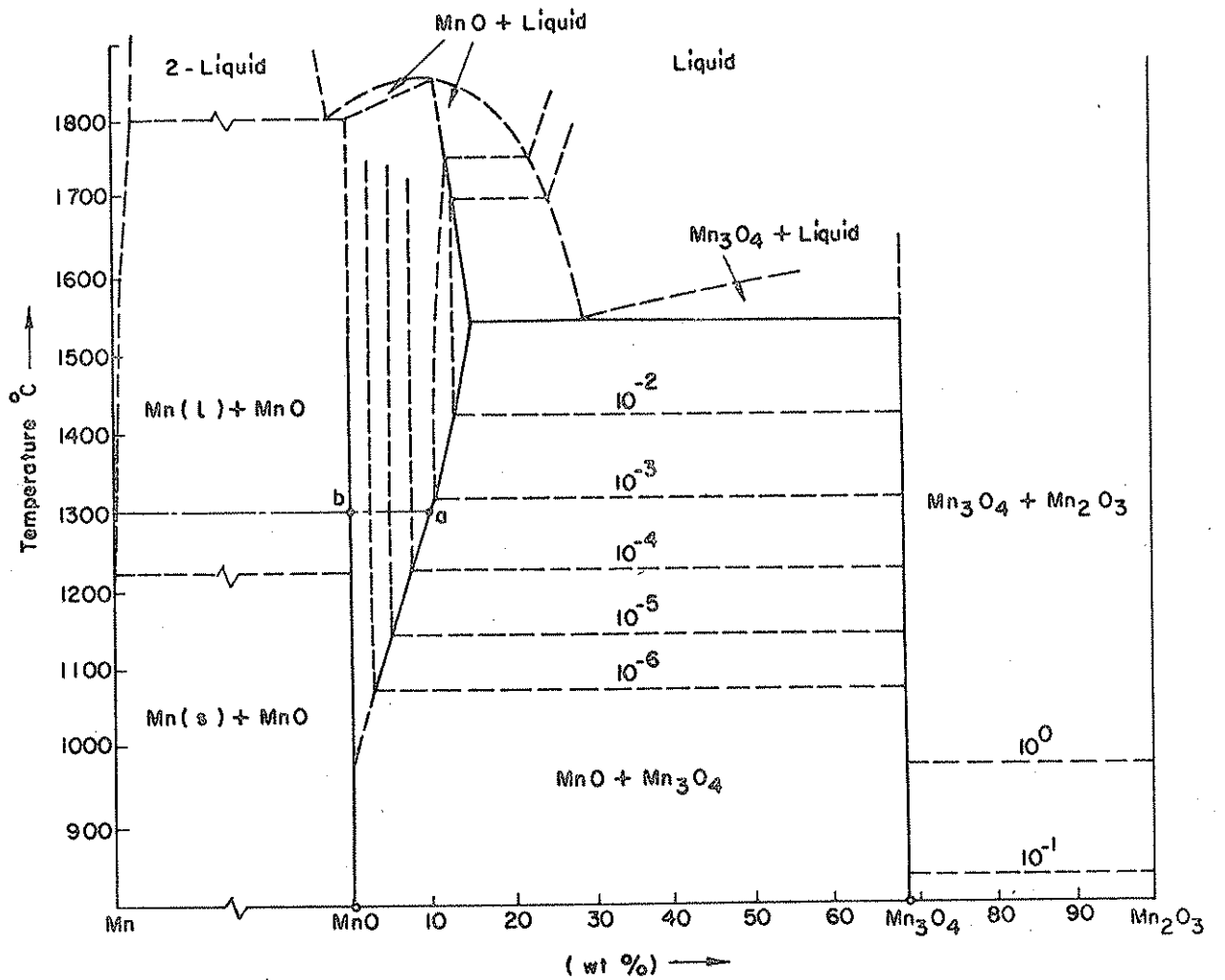


Figure 2 : The phase diagram for the system Mn-O between Mn and Mn₂O₃ compositions. After Phillips and Muan.⁶

oxygen for the coexistence of MnO and Mn is 1.45×10^{-18} atm.⁷

2.2. The Ni-O System

Phase relations between nickel and oxygen were investigated by Bogatski.⁸ The phase diagram shows that NiO is stoichiometric at all temperatures up to its melting point of 1960°C.

The conditions for the coexistence of metallic nickel and nickel oxide were studied by Hahn and Muan⁹ in the temperature interval 1100° to 1400°C. For the equilibrium reaction:



Hahn and Muan⁹ obtained:

$$\log P_{\text{O}_2} \text{ (atm)} = + 9.043 - \frac{24730}{T} \quad (2)$$

Thus, the standard free energy of formation of NiO can be expressed by:

$$\Delta G^\circ = - 236802 + 86.61 T \text{ J/gfw.} \quad (3)$$

Tretjakow and Schmalzried¹⁰ determined the standard free energy change of Reaction (1) in the interval 1000 - 1500 K by solid electrolyte emf studies; their results were expressed by the equation:

$$\Delta G^{\circ} = - 234625 + 85.39 T \quad \text{J/ gfw} \quad (4)$$

Steele, and more recently Davies and Smeltzer¹² conducted emf measurements on Reaction (1) using solid electrolyte galvanic cells. The standard free energy equations resulting from these studies yield ΔG° values within ± 250 J/gfw of those calculated from Equations (3) and (4) at 1300°C.

2.3. (The MnO - NiO System:

Most of our thermodynamic information on solid solutions of numerous oxide systems has been accumulated by the pioneering work of Muan^(*) and co-workers in this field within the past 20 years. The MnO - NiO solid solutions were among the first model systems in which the activities of NiO were determined by Hahn and Muan⁹ as early as 1961. Their measurements were carried out by gas-equilibration (methods and the activities of NiO were obtained in the temperature range 1100° to 1300°C as shown in Fig. 3.

Following the work of Hahn and Muan, two papers have been published bringing the results of solid state galvanic cell studies on this system into attention. Seetharaman and Abraham¹³ used a ThO₂-Y₂O₃ solid electrolyte to measure NiO activities in MnO - NiO solid solutions at 827°, 927° and 1027°C. Shortly after this work Cameron and

(*) Arnulf Muan: Formerly Professor of Metallurgy, now Professor of Mineral Sciences; The Pennsylvania State University, USA.

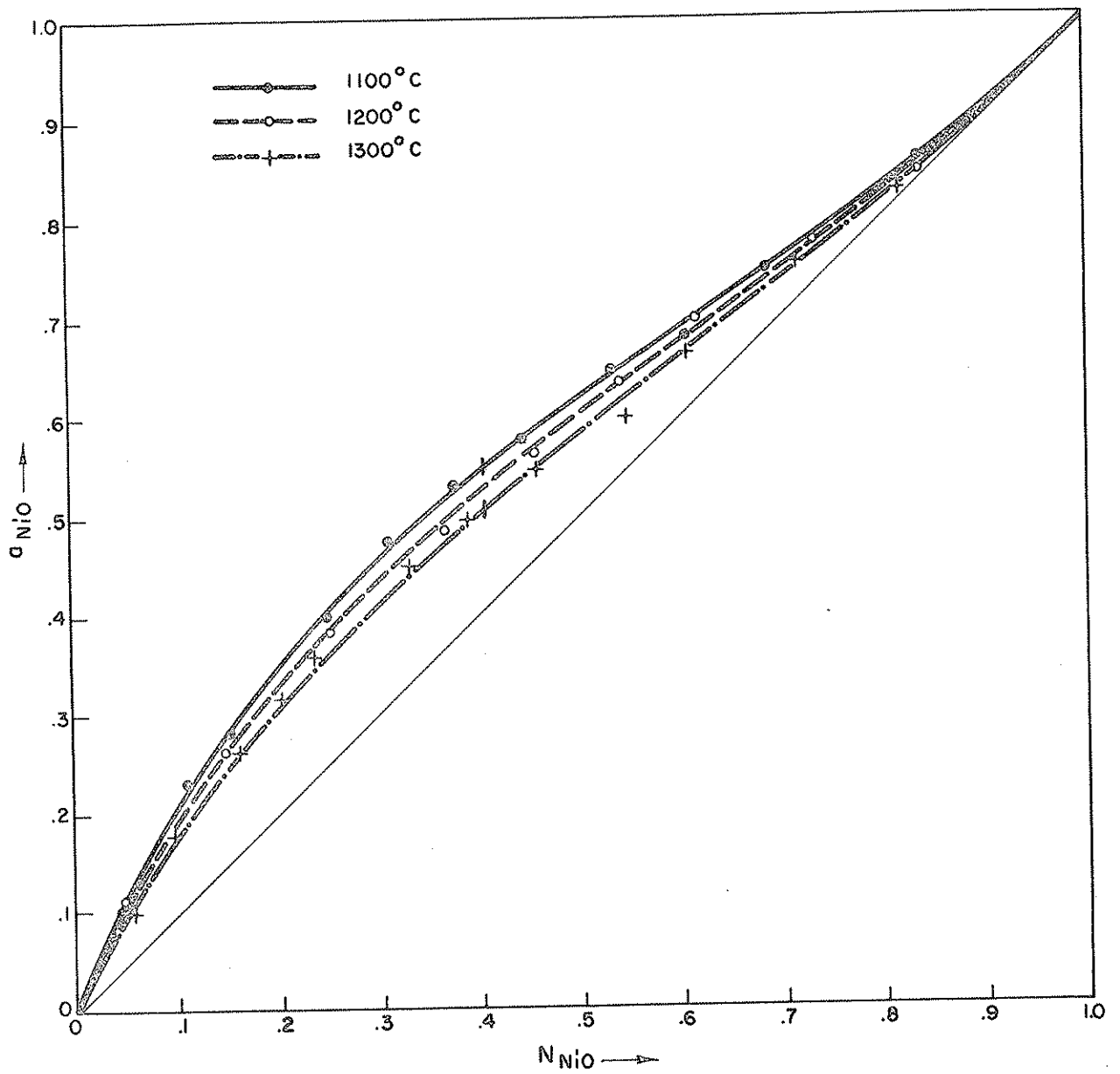


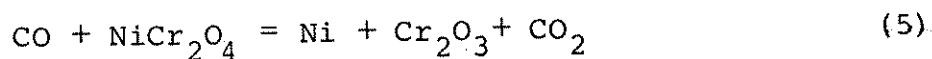
Figure 3 : Activity - Composition relations in MnO - NiO solid-solutions. After Hahn and Muan⁹.

Unger¹⁴ reported their emf results at 900°, 1000°, 1100°, and 1200°C obtained from cells using CaO - ZrO₂ solid electrolyte. Both emf studies confirmed the positive departures from ideality illustrated in Fig.3; furthermore, in general, the NiO activities of Cameron and Unger¹⁴ were in good agreement with those of Hahn and Muan⁹ particularly at 1200°C.

2. 4. The Systems NiO-Cr₂O₃ and MnO-Cr₂O₃.

The phase diagrams of the system NiO-Cr₂O₃ and MnO-Cr₂O₃ are not known; previous studies on these systems were confined to the measurement of the stabilities of NiCr₂O₄ and MnCr₂O₄ which happen to be the members of the above system. In connection with these studies, it has been established that, in the solid state, the mutual solubilities of NiO and Cr₂O₃, and MnO and Cr₂O₃ are negligible.

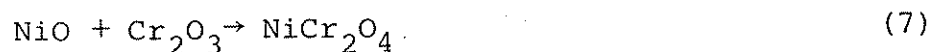
Several studies are made to determine the standard free energy of formation of NiO.Cr₂O₃ either by emf methods or by gas equilibration techniques. Kunmann, Rogers, and Wold¹⁵ measured the equilibrium CO/CO₂ ratios for the reaction:



Their data, obtained in the temperature range 1073-1380 K, could be converted into the expression:

$$\Delta G^\circ = - 98438 + 60.92 T \quad \text{J/gfw} \quad (6)$$

which gives the standard free energy of formation of $\text{NiO} \cdot \text{Cr}_2\text{O}_3$ from NiO and Cr_2O_3 according to the following reaction:



For Reaction (7), the emf studies of Tretjakow and Schmalzried¹⁰ yielded:

$$\Delta G^\circ = -54125 + 21.64 T \quad (400) \quad \text{j/gfw} \quad (8)$$

Equation (8) is specified¹⁰ to be valid at temperatures between 1000 to 1500 K. For the same reaction, Levitskii, Rezukhina, and Dneprova¹⁶ obtained from emf measurements:

$$\Delta G^\circ = -73464 - 4.48 T \quad \text{J/gfw.} \quad (9)$$

Lenev and Novakbatskii¹⁷ investigated the equilibrium CO/CO_2 ratios for Reaction (5) in the temperature range $900^\circ - 1200^\circ\text{C}$. Their data yields the following ΔG° expression for Reaction (7):

$$\Delta G^\circ = -51212 + 6.23 T \quad \text{J/gfw.} \quad (10)$$

Most recent data on the standard free energy of formation of $\text{NiO} \cdot \text{Cr}_2\text{O}_3$ from NiO and Cr_2O_3 comes from the emf measurements of Davies and Smeltzer.¹¹ Their tabular data in the interval $900^\circ - 1100^\circ\text{C}$ can be expressed by the following linear regression equation:

$$\Delta G^\circ = -61400 + 23.02 T \quad \text{J/gfw.} \quad (11)$$

Various equations available for ΔG° of $\text{NiO} \cdot \text{Cr}_2\text{O}_3$ as described above are displayed graphically in Figure 4. This figure shows clearly that the data on ΔG° are in gross conflict.

In contrast to the abundance of data on ΔG° of NiCr_2O_4 , the standard free energy of formation of MnCr_2O_4 has remained virtually unknown until Jacob and Fitzner¹⁸ reported a value of -59065 J/gfw at 1100°C for this quantity. This value represents an indirect estimate obtained from a study of equilibria between CoO-MnO and $\text{CoCr}_2\text{O}_4\text{-MnCr}_2\text{O}_4$ solid solutions.

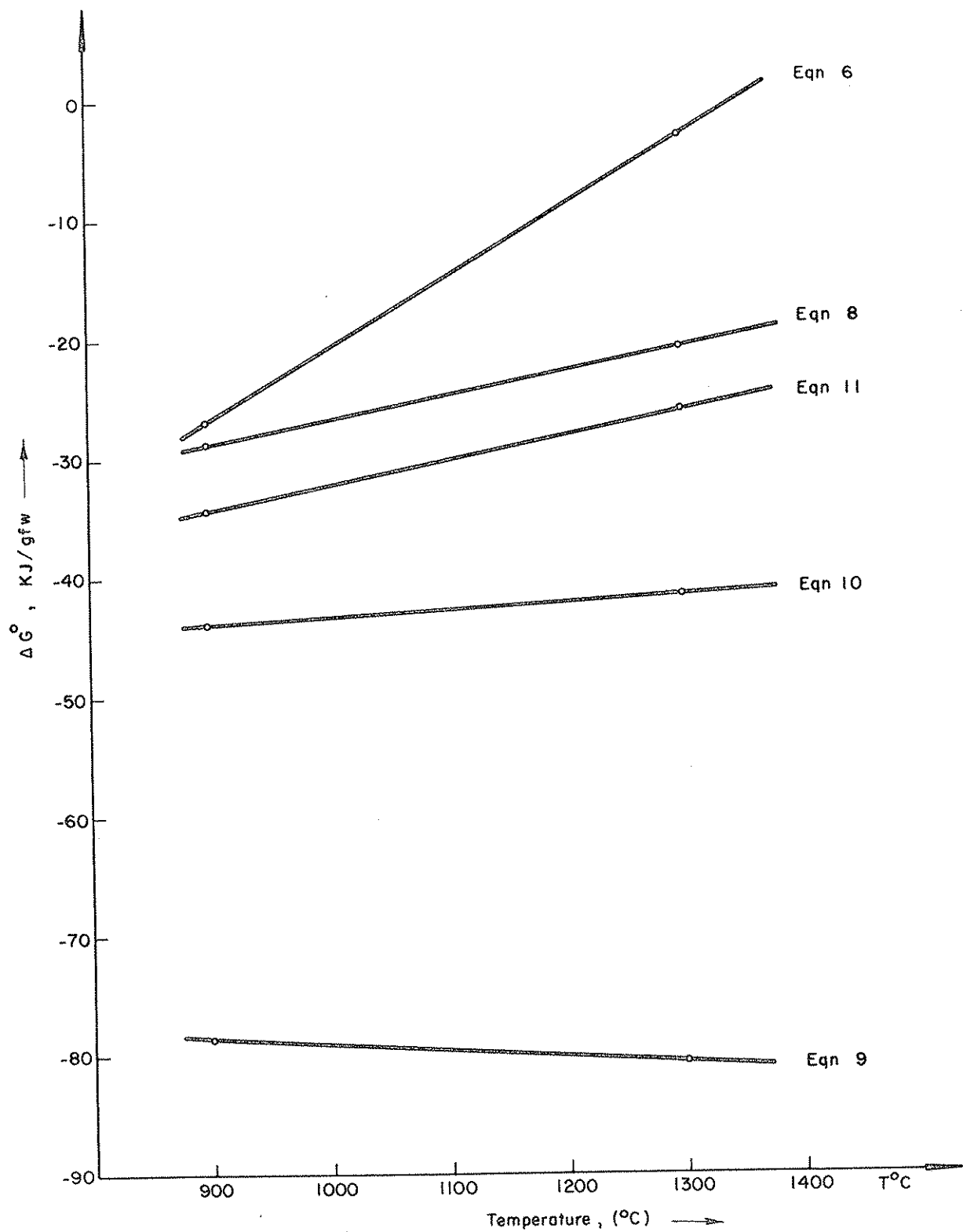


Figure 4 : The standard free energy of formation of $\text{NiO} \cdot \text{Cr}_2\text{O}_3$ from NiO and Cr_2O_3 (See text for the equations.)

CHAPTER III
EXPERIMENTAL PROCEDURE

3.1 Outline of the Experimental Procedure:

Numerous samples belonging to the system MnO-NiO-Cr₂O₃ were prepared by mixing the powders Cr₂O₃, Mn₃O₄, and NiO in desired proportions and sintering the pellets of these mixtures at elevated temperatures under controlled oxygen partial pressures. This preliminary treatment converted Mn₃O₄ to MnO and allowed to obtain partially homogenized starting samples of the MnO-NiO-Cr₂O₃ ternary.

For determination of conjugation lines between (Mn,Ni)O solid solutions and (Mn,Ni)Cr₂O₄ solid solutions at 1300°C the samples having these phase assemblages were equilibrated with a gas phase of known P_{O₂}. After equilibrium was reached, these two-phase samples were quenched to room temperature. The compositions of the conjugate phases were determined by X-ray diffraction analyses performed on the quenched samples. This same procedure was applied for the estimation of the phase boundaries, the X-ray analyses in this case being supplemented with microscopic examinations of the polished sections of the samples.

The activities of NiO in samples belonging to MnO - NiO, NiO - Cr₂O₃, MnCr₂O₄ - NiCr₂O₄ joins, and also in samples within the non-stoichiometry area of chromite solid solutions were established by determining the partial pressure of oxygen at which metallic nickel precipitates from members of these systems. The mixtures of CO₂ and H₂ or CO₂ and CO were used to generate the necessary oxygen potentials over the samples.

3.2 Details

3.2.1. Starting Oxides:

The oxides that were used in sample preparation and their characteristics were as follows.

a- Chromium Oxide: Analytical grade reagent powder of BDH chromic oxide was the source of Cr₂O₃. The manufacturer disclosed the existence of following impurities in the powder:

Chloride : 0.01 wt. pct max.

Sulphate : 0.20 wt pct max.

Water soluble matter : 0.20 wt pct max.

Loss at 600°C : 0.50 wt pct max.

Chromium oxide of specifications indicated above was heated at 700°C for 12 hours in a platinum crucible. Thus the volatiles and any free H₂O that could be present were

driven off and the purity of Cr_2O_3 was improved to better than 99.5 wt pct prior to its use.

b- Manganese Oxide: The source of MnO was Mn_3O_4 which, in turn, was obtained by thermal decomposition of the commercially available manganous oxide MnO_2 . The Riedel-de Haen AG manganese dioxide powder was specified to have the following maximum limits of impurities:

Chloride : 0.04 wt. pct.

Sulphate : 0.01 wt. pct.

Iron : 0.03 wt. pct.

In order to obtain Mn_3O_4 from MnO_2 , manganese dioxide powder was placed in a platinum crucible and heated in a muffle furnace at 1100°C for 24 hours. The resulting sintered mass of Mn_3O_4 was crushed and ground to -100 mesh after cooling it to room temperature.

c- Nickel Oxide : NiO was obtained by heating Riedel-de Haen AG black nickel oxide powder in a platinum crucible at 1000°C for 12 hours. The black color of the nickel oxide powder comes from Ni_2O_3 ; when nickel oxide is processed as described above Ni_2O_3 decomposes and the whole mass becomes green NiO. The NiO obtained by this treatment is a loosely sintered mass and can be used directly without any preliminary grinding. No specifications are given for the impurities present in the starting nickel oxide powder; a spectrographic analysis performed on green NiO revealed the existence of very weak lines for Fe. Thus,

the starting NiO could be accepted as an analar reagent.

3.2.2. Preparation of Oxide Mixtures:

Oxide samples of desired compositions were prepared by weighing the powders Cr_2O_3 , NiO, and Mn_3O_4 in calculated proportions. These powders were mixed by grinding them under acetone in an agate mortar. In order to obtain a homogenous distribution, the mixing time was kept rather long, i.e., 30 minutes. When the acetone has evaporated completely, the mixtures were pressed under a load of 6000 kg/cm^2 into dense cylindrical pellets 1 cm. in diameter.

Each pellet was placed in a platinum crucible and heated in air at 1100°C for 48 hours in a muffle furnace. This treatment resulted in reactions to occur between NiO and Cr_2O_3 so that NiO - NiO. Cr_2O_3 phase assemblages would develop. The mixtures containing Mn_3O_4 received an additional thermal treatment. These pellets, after prereacting in air at 1100°C , were heated at 1300°C in a vertical tube furnace for 12 hours, each under a controlled atmosphere having a partial pressure of oxygen $P_{\text{O}_2} = 10^{-6}$ atm. This atmosphere was generated by a $\text{CO}_2 - \text{H}_2$ gas mixture, the induced oxygen pressure was sufficiently low to reduce Mn_3O_4 to MnO but it was oxidizing enough not to cause any precipitation of metallic nickel. The two thermal treatments described

above allowed Cr_2O_3 , NiO , and MnO react to yield homogenized pellets which served as the starting samples in the subsequent equilibration runs.

3.2.3. Equilibration Experiments:

The equilibration experiments consisted of reacting portions of the previously homogenized pellets with a gas phase of known oxygen partial pressures. During an equilibration run, the oxide sample exchanges oxygen with the gas phase. The duration of each run was kept sufficiently long so that these exchange reactions would cease and the phases present in the sample would adjust their compositions corresponding to the equilibrium state. The pieces of the experimental set-up involved in equilibration runs and the procedures related thereof are described in the following sections.

3.2.3.1. Equilibration Furnace:

A vertical tube furnace was used to perform the equilibration experiments at a constant temperature of 1300°C . The furnace was heated by a helical Crusilite element capable of reaching 1500°C . The reaction chamber, a mullite tube, was inserted into the hollow space of the heating element, a pyrex glass joint with a side

arm for gas admission was cemented to the bottom of the furnace tube. The female half of the pyrex joint was shaped into a quench cup, this part carried a U-tube glass extension for admitting the quenching water.

The furnace was powered from an external electrical circuit, the basic units of which were a Variac and a Pye-Ether Digi temperature controller. One leg of the Crasilite element was connected to the variac outlet and the other leg was connected to the outlet of the controller. The controller, coupled to a thyristor, was actuated with the aid of a Pt-Pt 13 pct Rh thermocouple. This power and control circuit allowed to maintain the temperature constant in the furnace tube within $\pm 2^{\circ}\text{C}$.

3.2.3.2. Gas Atmospheres:

The gaseous atmospheres with controlled oxygen partial pressures were obtained by using metered mixtures of CO_2 and CO gases. A single cylinder of Matheson CP grade CO was available at the beginning of the experiments; when this cylinder was emptied H_2 gas replaced CO in CO_2 - CO mixtures.

The equilibrium between CO, CO_2 and O_2 can be described by:



The equilibrium constant for the above reaction is $K = 10^{4.844}$, at 1300°C ,¹⁹ Hence from the expression:

$$K = \frac{P_{\text{CO}_2}}{P_{\text{CO}} \cdot \sqrt{P_{\text{O}_2}}} \quad (13)$$

we obtain:

$$\sqrt{P_{\text{O}_2}} = 10^{-4.844} \cdot \left(\frac{P_{\text{CO}_2}}{P_{\text{CO}}} \right) \quad (14)$$

Equation (14) enables to calculate the $\frac{\text{CO}_2}{\text{CO}}$ ratios which will generate well defined P_{O_2} values in the reaction chamber.

The calculation of the proportions in which CO_2 and H_2 should be mixed in order to obtain a specific P_{O_2} is a little more complicated. Consider the reaction:



At 1300°C , the equilibrium constant for Reaction (15) is¹⁹ $K = 10^{0.464}$. Hence, from:

$$K = \frac{P_{\text{CO}} \cdot P_{\text{H}_2\text{O}}}{P_{\text{CO}_2} \cdot P_{\text{H}_2}} \quad (16)$$

We have:

$$\frac{P_{\text{CO}} \cdot P_{\text{H}_2\text{O}}}{P_{\text{CO}_2} \cdot P_{\text{H}_2}} = 10^{0.464} \quad (17)$$

Assume that (r) moles of CO_2 and 1 mole of H_2 are mixed initially, so that the initial mixing ratio is denoted by:

$$r = \frac{\text{CO}_2}{\text{H}_2}$$

At equilibrium, if (x) mole of CO forms from this mixture, (x) mole of H_2O also form according to the stoichiometry of Reaction (15). Thus, in the equilibrium mixture, the number of moles of each gas and the corresponding partial pressures at $P_T = 1$ atm will be:

$$\begin{aligned} n_{\text{CO}_2} &= r - x \text{ mole,} & P_{\text{CO}_2} &= \frac{r - x}{r + 1} \text{ atm,} \\ n_{\text{H}_2} &= 1 - x \text{ mole} & P_{\text{H}_2} &= \frac{1 - x}{r + 1} \text{ atm,} \\ n_{\text{H}_2\text{O}} &= x \text{ mole,} & P_{\text{H}_2\text{O}} &= \frac{x}{r + 1} \text{ atm,} \\ n_{\text{CO}} &= x \text{ mole,} & P_{\text{CO}} &= \frac{x}{r + 1} \text{ atm.} \end{aligned}$$

When the expressions for partial pressures are inserted into Equations (14) and (17), upon rearrangement, we obtain the following set:

$$r = (1 + 10^{4.844} \sqrt{P_{\text{O}_2}}) x \quad (18)$$

$$\sqrt{P_{O_2}} = \frac{x}{10^{5.308} (1-x)} \quad (19)$$

For a desired P_{O_2} , first, x is solved from Equation (19) and then r is evaluated from Equation (18) by using the $(\sqrt{P_{O_2}}, x)$ combination of the previous step.

In order to obtain $CO_2 - CO$ and $CO_2 - H_2$ gas mixtures of definite compositions a gas mixer similar to the one described by Darken and Gurry¹⁹ was used. This device, shown in Figure 5 contains two differential manometers; each manometer has a levelling bottle which adjusts the height of the manometer fluid. The open ends of a manometer are connected with a removable capillary tube. The levelling bottle and its extensions are filled with aqueous copper sulfate. The flow-rate is a function of both the manometer height and the diameter of the capillary tube attached to the open ends of the U-tube. The flow rate is kept constant at any desired value by clamping the levelling bottle to a vertical rod and letting the excess of the gas escape through the bleeder tube.

The individual capillaries for CO_2 , CO , and H_2 gases were calibrated against manometer heights by the soap-bubble column method. A vertical 50 cc capacity burette with a soap reservoir at the bottom was used for this purpose. The time necessary for the gas to pick up a bubble and travel through 40 cc volume permitted calculation

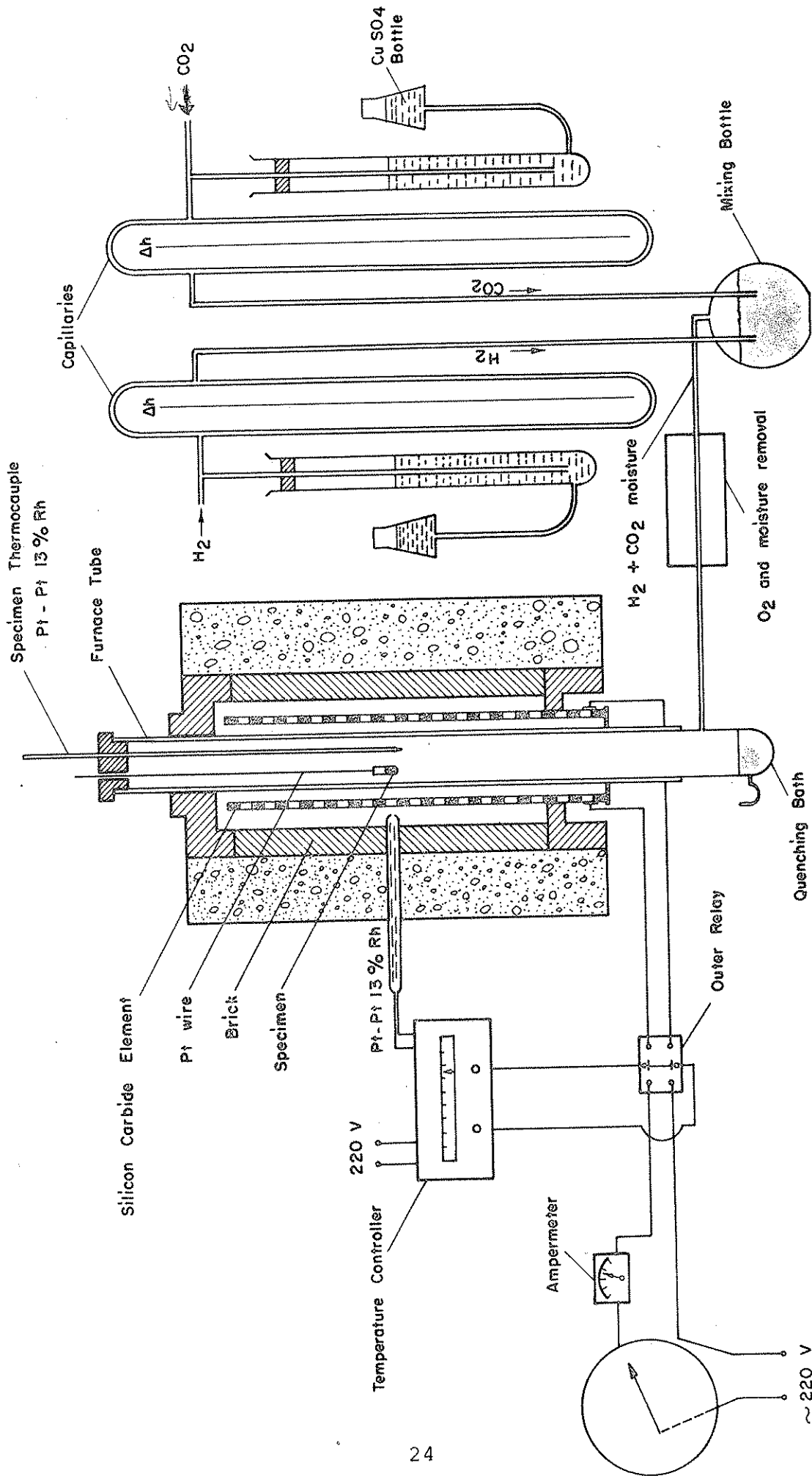


Figure 5 : Position of furnace, specimen and gas mixing system.

of the flow rate in cc/sec. Figures 6,7,8, and 9 show flow rate charts for the individual gases.

The gases CO_2 , CO , and H_2 were purified from their oxygen by passing them through a column of copper chips heated to 500°C . The moisture in the gases were eliminated by passing them over Drierite. The gases coming from individual manometers are mixed in a glass chamber filled with glass wool. The gas mixture was fed to the furnace tube from bottom.

3.2.3.3. Equilibration Runs

For an equilibration run, the fragments of previously reacted pellets were placed in a Pt crucible and suspended into the hot zone of the equilibration furnace by a thin Pt wire. The top of the furnace tube was covered by a refractory lid with a hole for sample suspension and an additional hole for admitting the sample thermocouple. The flow rates of the gas mixtures were adjusted within 1-1.5 cc/sec so that the effects of thermal segregation would be eliminated.

The duration of an equilibration run was about 8 hours. This was much longer than the time necessary to reach equilibrium; in the preliminary experiments it has been established that nickel precipitation could occur

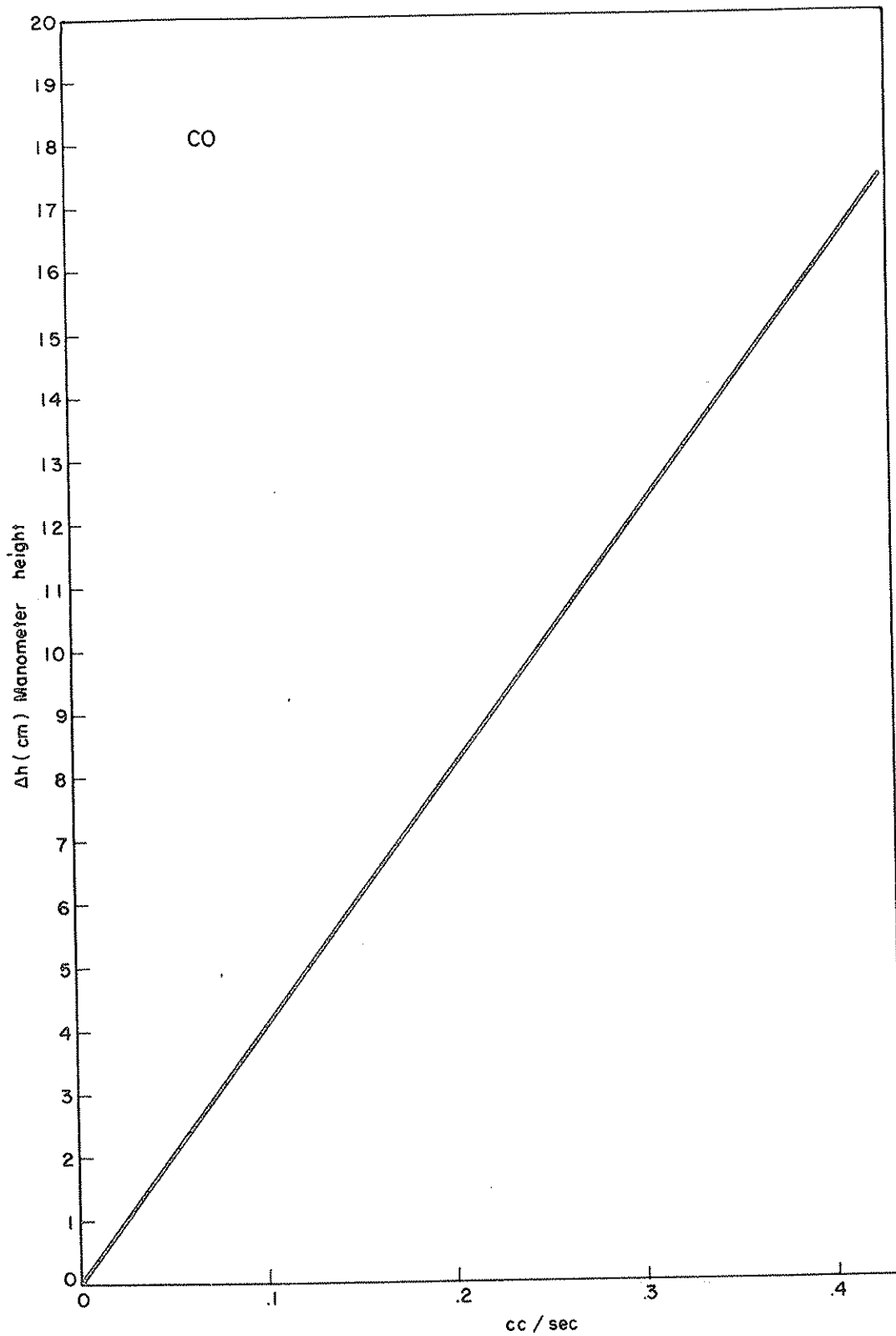


Figure 6 : The flow rate calibration curve of CO capillary.

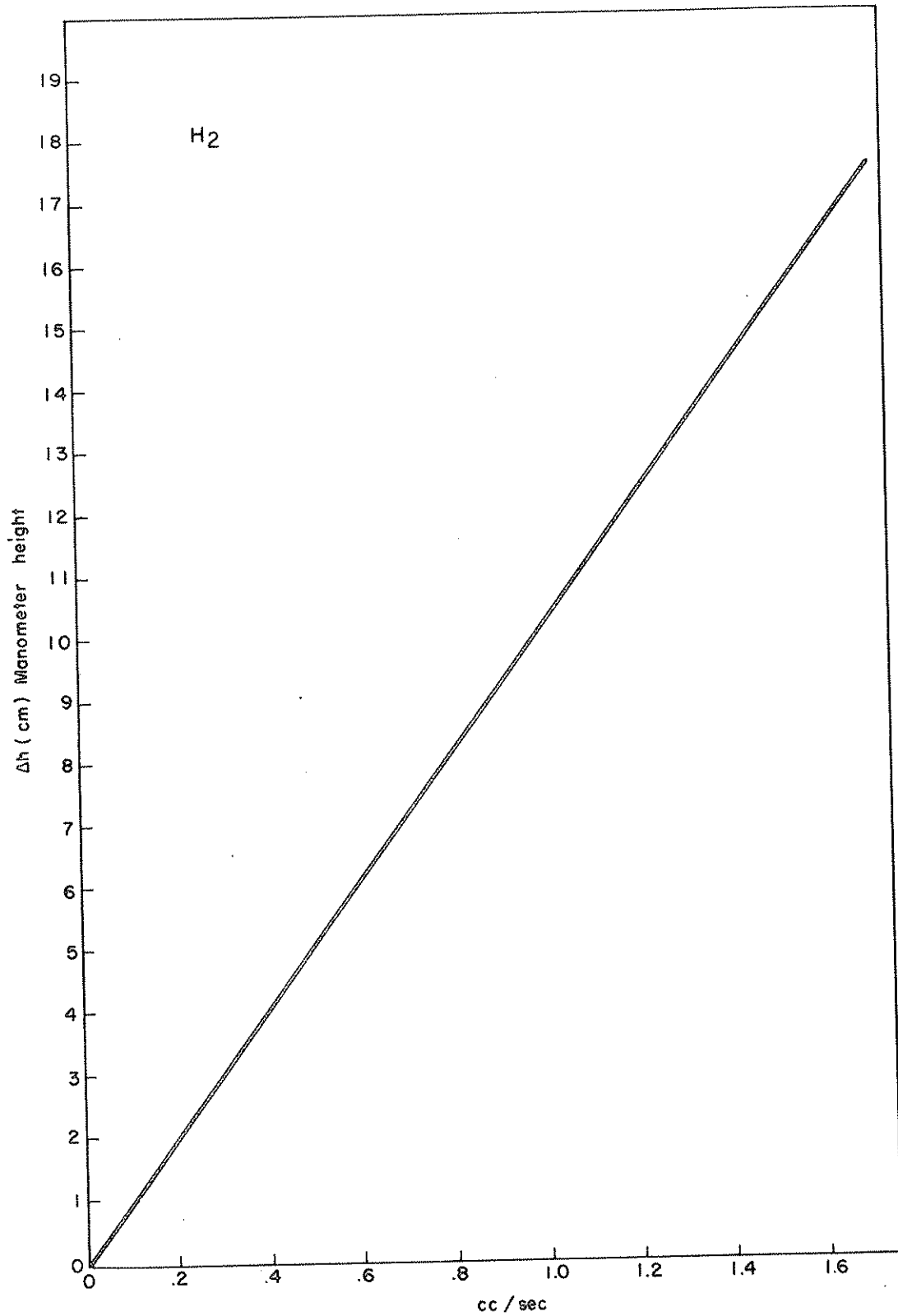


figure 7 : The flow rate calibration curve of H₂ capillary.

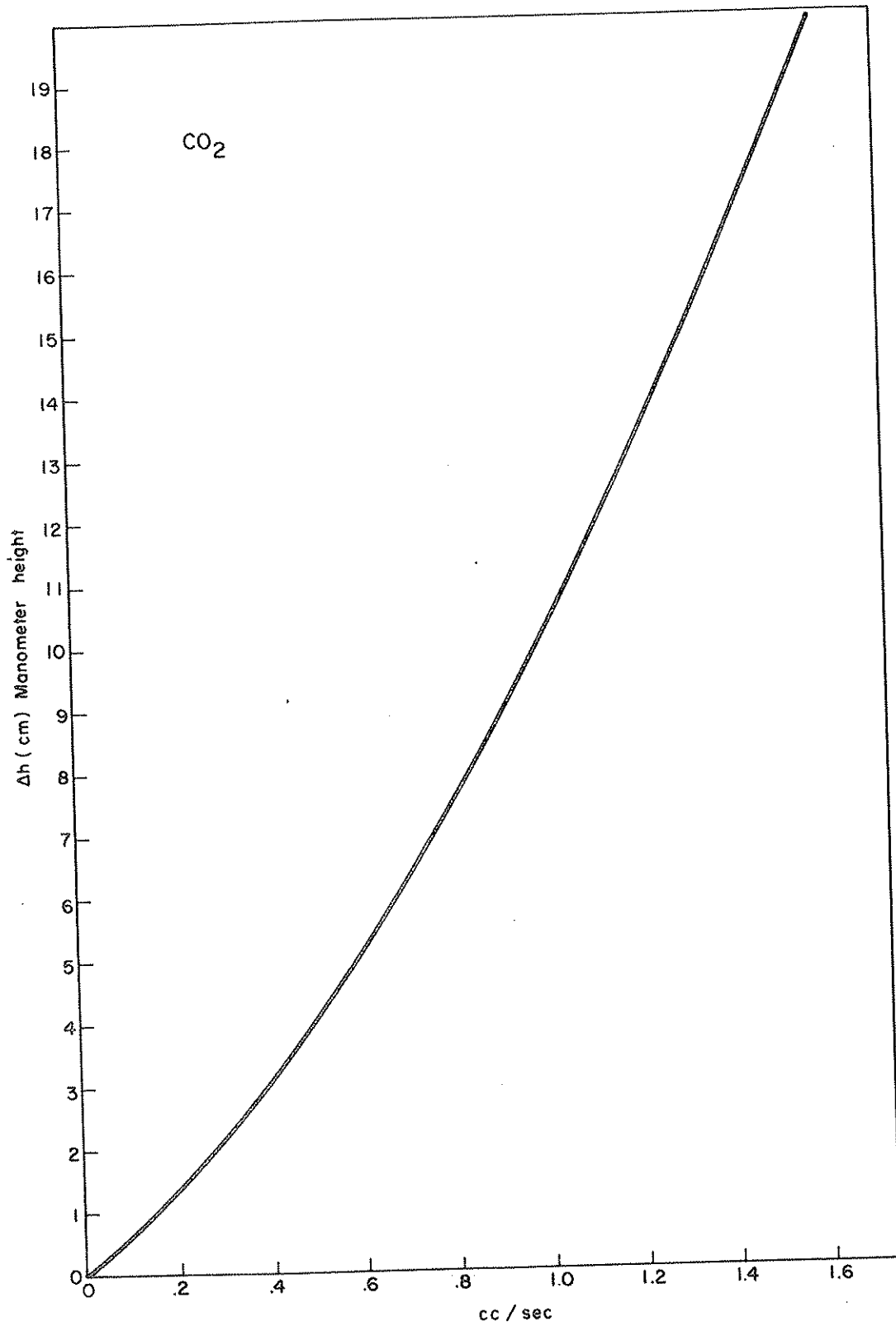


Figure 8 : The flow rate calibration curve of CO₂ capillary.

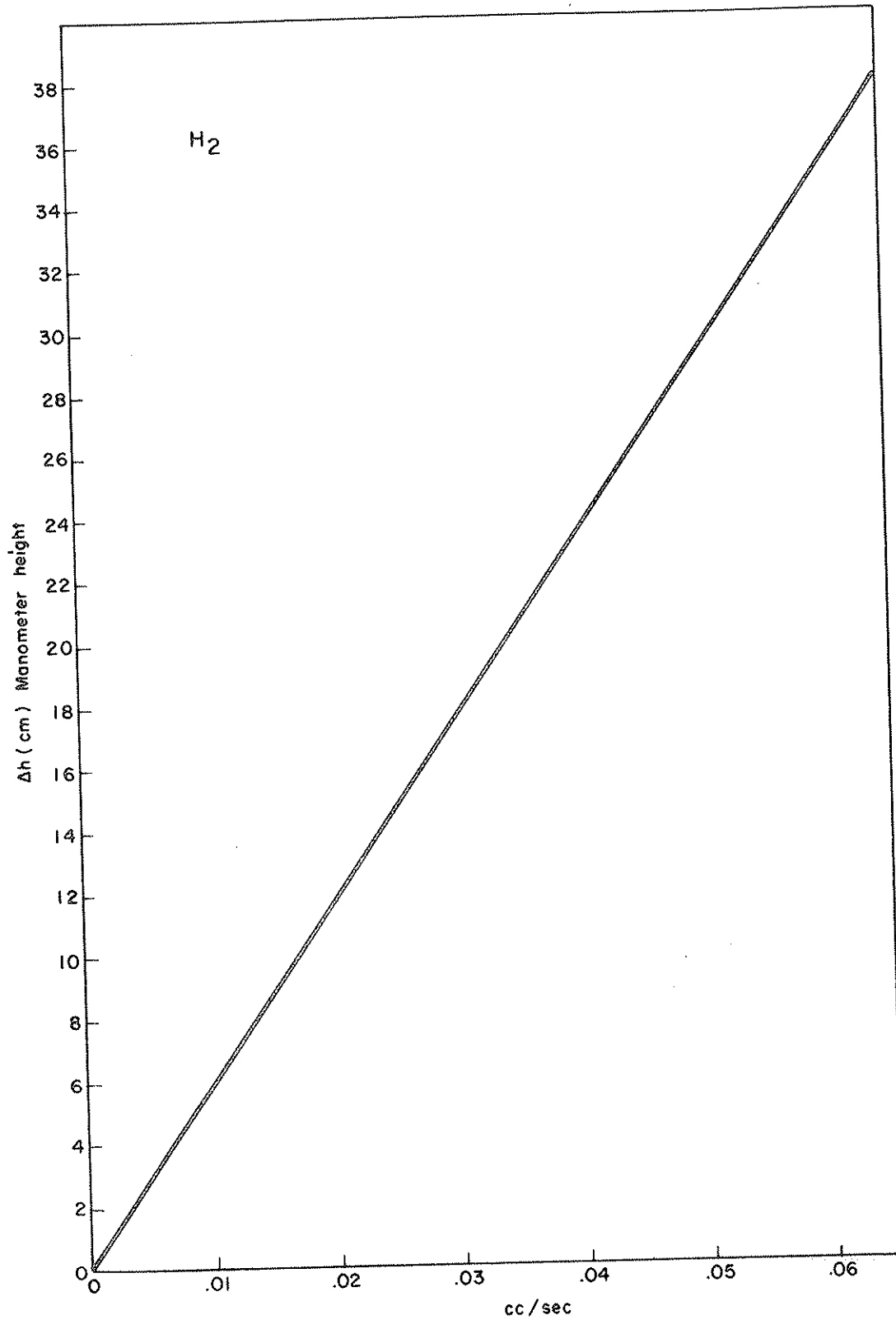


Figure 9 : The flow rate calibration curve of H₂ capillary.

within the first 3 hours of equilibration. The relatively short equilibration time was evidently due to the homogenization of the pellets under reducing conditions in the sample preparation stage.

The temperatures within the furnace tube were measured at regular intervals by a standardized Pt-Pt 13 % Rh thermocouple. At the end of an equilibration run, the sample was cooled quickly to room temperature by dropping it into water contained in the quenching cup at the bottom of the furnace tube.

3.2.3.4. Sample Examination:

Phase identifications in quenched samples were done by examining their polished sections under microscope. For this purpose, portions of the samples were mounted in epoxy resin and the sections were prepared by conventional metallographic techniques. No etching was necessary since the difference between the reflectivities of various phases permitted their identification easily. The samples belonging to the spinel + oxide phase assemblage field were subjected to x-ray diffraction analyses. These analyses were aimed primarily at determining the location of d_{200} peaks of oxide solid solutions, so that their compositions would be ascertained with reference to a previously known d_{200} versus composition chart.

CHAPTER IV

DATA and RESULTS

The data obtained in equilibration experiments and the thermodynamic calculations performed through their use are presented in the following sections.

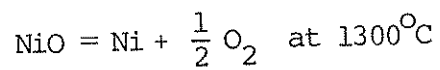
4.1. The Ni-NiO Equilibrium

The equilibrium between metallic nickel and nickel oxide was expressed in Section 2.2 by the reaction :



In the present study the partial pressure of oxygen which satisfies the equilibrium Reaction (1) at 1300°C has been determined by subjecting a pure NiO pellet to the reducing action of CO₂-H₂ gas mixtures. The conversion of nickel oxide to metallic nickel could be observed either by polishing the quenched sample or directly by naked eye. The results are given in Table I. As would be seen from this table a gas mixture having the ratio $r = \frac{\text{CO}_2}{\text{H}_2} = 32.50$ results in the coexistence of Ni + NiO ; hence this represents the equilibrium gas. The partial pressure of oxygen corresponding to this specific ratio is $P_{\text{O}_2} = 10^{-6.6742}$ atm as calculated from Equations (18) and (19). The value of

TABLE I : Critical runs for the determination of the equilibrium

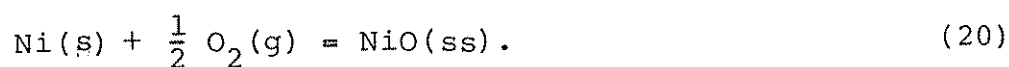


Specimen composition	$r = \frac{\text{CO}_2}{\text{H}_2}$	$-\log P_{\text{O}_2}$	Present Phases
NiO	32.91	6.6037	NiO
NiO	32.50	6.6742	NiO + Ni (trace)
NiO	31.94	6.6961	Ni

P_{O_2} obtained from the data of Hahn and Muan⁹ (Equation 2) is $10^{-6.6786}$ atm. The very good concordance of two P_{O_2} values can be taken as an indication of the fact that the present set up will produce accurate data on equilibrium gas ratios, and hence accurate P_{O_2} values.

4.2. Activity-Composition Relations in MnO-NiO Solid Solutions

For a MnO-NiO solid solution of given composition the equilibrium between metallic nickel, oxygen, and oxide solid solution can be described by the reaction :



where the subscripts s,g,ss denote, respectively, the solid metal phase, gas, and the oxide solid solution.

The equilibrium constant for Reaction (20) is ;

$$K = \frac{a_{NiO}}{a_{Ni} P_{O_2}^{1/2}} . \quad (21)$$

In the pure Ni-O system the activities of NiO and Ni are taken as unity, then :

$$K = \frac{1}{(P_{O_2}^*)^{1/2}} . \quad (22)$$

Combining Equations (21) and (22), we obtain for the activity of NiO :

$$a_{\text{NiO}} = \left(\frac{P_{\text{O}_2}}{P_{\text{O}_2}^*} \right)^{1/2} \quad (23)$$

Here, P_{O_2} represents the equilibrium partial pressure of oxygen for Reaction (20), and $P_{\text{O}_2}^*$ is $10^{-6.6742}$ atm at 1300°C . ✓

In the present work values of P_{O_2} for the equilibrium Reaction (20) were measured for some MnO-NiO solid solutions. This is done by subjecting the solid solutions selected to gas mixtures of decreasing $\frac{\text{CO}_2}{\text{H}_2}$ ratios until the precipitation of metallic nickel is observed. The results are tabulated in Table II, and are shown graphically in Figure 10 on the activity-composition plot for NiO. In general, the present NiO activities are in good agreement with the previously reported values.^{9,14} The NiO activities of Cameron and Unger¹⁴ were extrapolated to 1300°C by the procedure outlined in Appendix 1. The smooth NiO curve shown in Figure 10 is passed from the average of data points belonging to this work and those of earlier studies.^{9,14}

The corresponding MnO activities could be obtained by a Gibbs-Duhem treatment of a_{NiO} data using the following equation :

$$N_{\text{MnO}} \cdot d \log \gamma_{\text{MnO}} + N_{\text{NiO}} \cdot d \log \gamma_{\text{NiO}} = 0. \quad (24)$$

TABLE II : Activity measurements of NiO in the MnO - NiO System.

Sample Composition (mole fraction)		Measured	Equilibrium	Present	Nickel Oxide
N_{MnO}	N_{NiO}	$-\log P_{\text{O}_2}$	$-\log P_{\text{O}_2}$	Phases	Activity
0.80	0.20	7.6112		SS	
		7.6371		SS	
		7.6639		SS + Ni	
			7.6504		0.325 ± 0.002
0.65	0.35	7.0484		SS	
		7.3300		SS	
		7.3736		SS + Ni (trace)	
		7.3973		SS + Ni	
			7.3737		0.447 ± 0.002
0.50	0.50	7.1546		SS	
		7.1686		SS + Ni	
			7.1625		0.570 ± 0.003
0.30	0.70	6.9333		SS	
		6.9499		SS + Ni	
			6.9416		0.735 ± 0.004
0.27	0.73	6.8735		SS	
		6.9013		SS	
		6.9184		SS + Ni	
		6.9417		SS + Ni	
			6.9126		0.760 ± 0.004

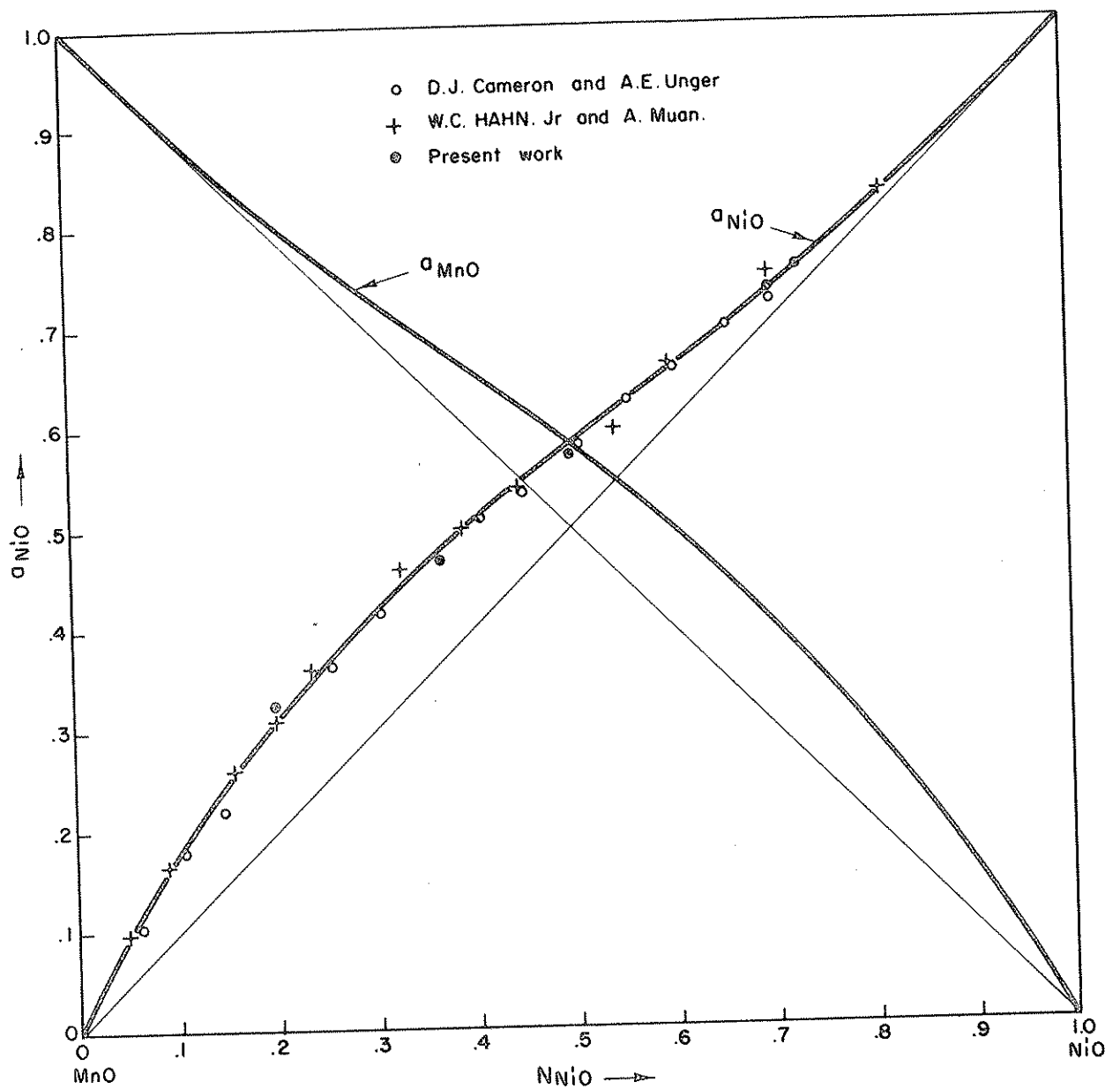


Figure 10 : Activity of NiO and MnO as a function of composition in the MnO - NiO system at 1300°C.

Activities of MnO were calculated by using Equations (27) and (28). The results are given in Table III, and are shown in Figure 10.

4.3. Determination of the Nonstoichiometric Region of Nickel Chromite and Activities of NiO and Cr_2O_3 in the Cr_2O_3 -NiO System.

As mentioned earlier in Section 2.4. the terminal solid solubilities of NiO in Cr_2O_3 and Cr_2O_3 in NiO are negligible. In the previous studies no attempts were made to establish whether or not NiCr_2O_4 is a perfectly stoichiometric compound. In the present work non-stoichiometry in NiCr_2O_4 is examined by measuring NiO activities in seven samples having the compositions indicated in Table IV. The activity of NiO in the exactly stoichiometric nickel chromite and in samples with more Cr_2O_3 than the stoichiometric NiCr_2O_4 composition is 0.255. In contrast when the NiO content increases above that in the stoichiometric formula, the activity of NiO increases sharply within a narrow composition interval as shown in Table V and in Figure 11. Following conclusions can be drawn from Figure 11:

1. Nickel chromite is a solid solution phase within the composition range $N_{\text{NiO}}=0.50$ to $N_{\text{NiO}}=0.53$. Hence NiCr_2O_4 can exist as a non-stoichiometric compound with an excess of NiO over the stoichiometric representation.

TABLE III : Activities of MnO in the MnO - NiO solid solutions.

Sample Composition (mole fraction)		$\alpha_{\text{NiO}} = \frac{\ln \gamma_{\text{NiO}}}{(1-N_{\text{NiO}})^2}$	γ_{MnO}	a_{MnO}
N_{NiO}	N_{MnO}			
0.10	0.90	0.662	1.0024	0.902
0.20	0.80	0.669	1.0171	0.814
0.30	0.70	0.627	1.0590	0.741
0.40	0.60	0.190	1.1078	0.664
0.50	0.50	0.340	1.1647	0.582
0.60	0.40	0.529	1.2726	0.509
0.70	0.30	0.512	1.3682	0.410
0.80	0.20	0.403	1.4983	0.299
0.90	0.10	0.443	1.6623	0.166

TABLE IV : Activities of nickel oxide as a function of composition along the NiO - Cr₂O₃ join at 1300°C

Samp. No.	Sample Composition (mole fraction)		Measured	Equilibrium	Present	Nickel Oxide
	N _{NiO}	N _{Cr₂O₃}	-log P _{O₂}	-log P _{O₂}	Phases	Activity
29	0.40	0.60	7.8352	7.8619	SS *	0.255±0.001
			7.8619		SS + Ni (trace)	
			7.9180		SS + Ni	
			7.9779		SS + Ni	
30	0.45	0.55	7.8352	7.8619	SS	0.255±0.001
			7.8619		SS + Ni (trace)	
			7.9180		SS + Ni	
31	0.48	0.52	7.6681	7.8619	SS	0.255±0.001
			7.7594		SS	
			7.8619		SS + Ni (trace)	
			7.9180		SS + Ni	
32	0.50	0.50	7.8352	7.8619	SS	0.255±0.001
			7.8619		SS + Ni (trace)	
			7.9180		SS + Ni	
			7.9779		SS + Ni	
			8.1121		SS + Ni	

(★) - Solid solution

TABLE IV : (Continued)

Samp. No.	Sample Composition (mole fraction)		Measured	Equilibrium	Present Phases	Nickel Oxide Activity
	N_{NiO}	$N_{Cr_2O_3}$	$-\log P_{O_2}$	$-\log P_{O_2}$		
33	0.51	0.49	6.7853		SS	
			6.8205		SS	
			6.8735		SS	
			6.9126		SS+Ni (trace)	
			6.9126			0.760±0.004
34	0.52	0.48	6.7139		SS	
			6.7433		SS	
			6.7738		SS+Ni (trace)	
			6.7738			0.892±0.005
35	0.54	0.46	6.6737		SS	
			6.6742		SS+Ni (trace)	
			6.6961		SS+Ni	
			6.7416		SS+Ni	
			6.7510		SS+Ni	
			6.6742			1.000±0.005

TABLE V : Activities of NiO and Cr₂O₃ in nickel chromite solutions

a_{NiO}	N_{NiO}	$-\log a_{\text{NiO}}$	$\frac{n_{\text{NiO}}}{n_{\text{Cr}_2\text{O}_3}}$	$-\log a_{\text{Cr}_2\text{O}_3}$	$a_{\text{Cr}_2\text{O}_3}$
0.255	0.500	0.5935	1.000	0	1.000
0.340	0.501	0.4685	1.004	0.1255	0.749
0.600	0.505	0.2218	1.024	0.3755	0.421
0.760	0.510	0.1192	1.0408	0.4813	0.330
0.900	0.530	0.04575	1.0833	0.5591	0.276
1.000	0.540	0	1.1276	0.6097	0.246

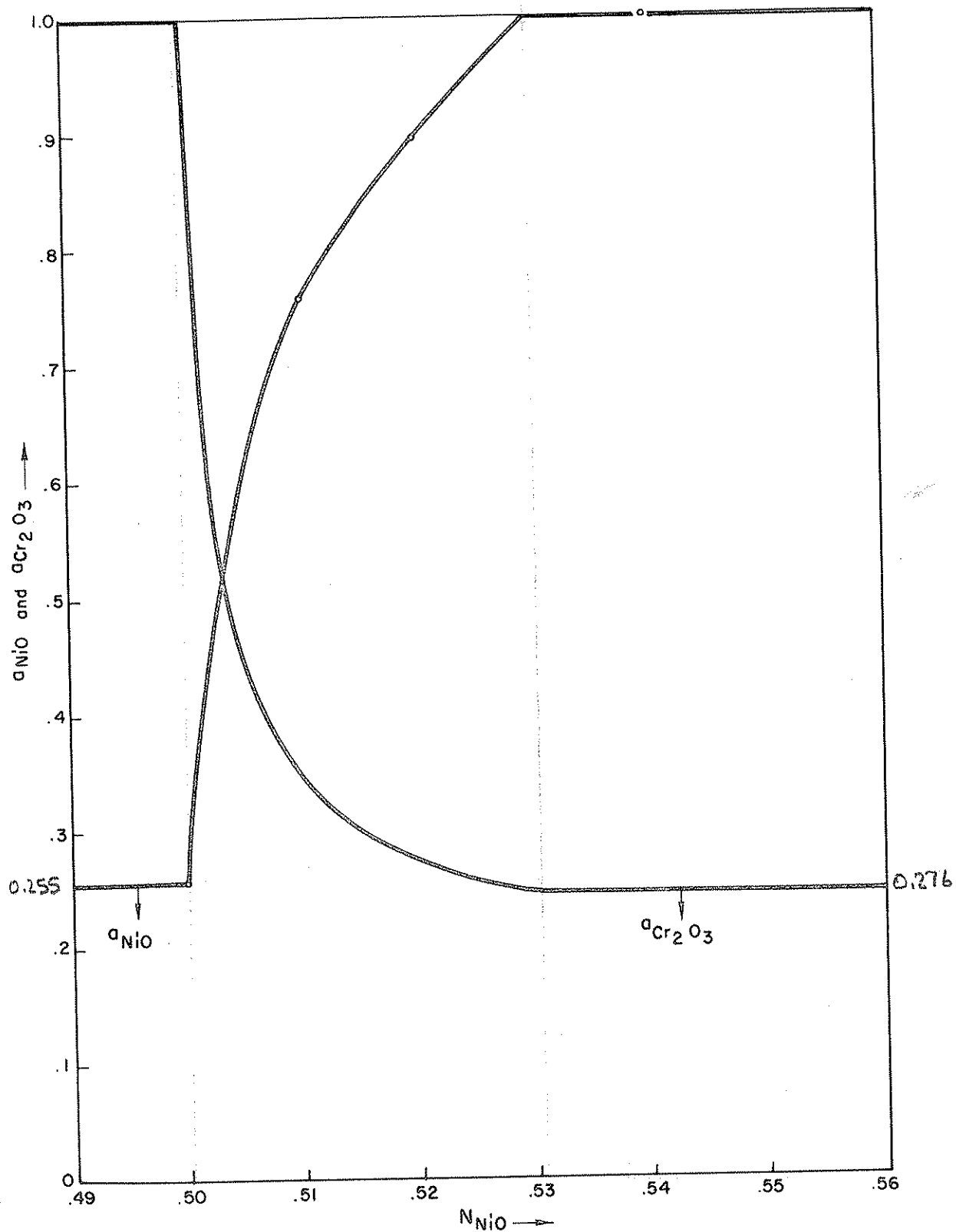


Figure 11 : Activity of NiO and Cr₂O₃ as a function of composition in NiO - Cr₂O₃ system.

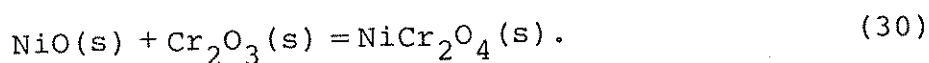
2. Exactly stoichiometric NiCr_2O_4 exists at 1300°C without any excess of Cr_2O_3 .

The Cr_2O_3 activities in the chromite solid solution can be obtained by a graphical integration of the following Gibbs-Duhem equation:

$$d\log a_{\text{Cr}_2\text{O}_3} = - \frac{n_{\text{NiO}}}{n_{\text{Cr}_2\text{O}_3}} d\log a_{\text{NiO}} \quad (29)$$

At the point where $\frac{n_{\text{NiO}}}{n_{\text{Cr}_2\text{O}_3}} = 1$, the activity of chromium oxide is unity. The results of the integration of Equation (29) are summarized in Table V and the variation of chromium oxide activities with respect to composition is shown in Figure 11.

The formation of NiCr_2O_4 from nickel oxide and chromium oxide is represented by the reaction:



The standard free energy change of Reaction (30) is given by:

$$\Delta G^\circ = -RT \ln \frac{a_{\text{NiCr}_2\text{O}_4}}{a_{\text{Cr}_2\text{O}_3} \cdot a_{\text{NiO}}} \quad (31)$$

At the exactly stoichiometric NiCr_2O_4 composition, $a_{\text{NiCr}_2\text{O}_4}$ and $a_{\text{Cr}_2\text{O}_3}$ are unity, so the standard free energy change can be written as:

$$\Delta G^{\circ} = RT \ln a_{\text{NiO}} \quad (32)$$

Activity of nickel oxide was measured as 0.255 (Table IV) hence, the standard free energy of formation of NiCr_2O_4 can be calculated as -17484.8 J/gfw. This represents the standard free energy of formation of NiCr_2O_4 from its oxide components NiO and Cr_2O_3 at 1300°C.

4.4. The Stability of Manganese Chromite at 1300°C

Similar to the situation for nickel chromite, the stability field of manganese chromite has not been examined in previous studies. In their work on the system $\text{CoO-MnO-Cr}_2\text{O}_3$ Jacob and Fitzner¹⁸ suggested that MnCr_2O_4 may have some excess of Cr_2O_3 over the stoichiometric formula. In order to establish the stability field of manganese chromite along the $\text{MnO-Cr}_2\text{O}_3$ join six samples were prepared and were equilibrated with a gas phase of $P_{\text{O}_2} = 10^{-8.18}$ atm for 32 hours at 1300°C. These samples were quenched to room temperature and the phases present in them were determined by x-ray diffraction and by metallographic examinations. The compositions of the samples studied and the results of phase identification are given in Table VI. In accordance with these results, MnCr_2O_4 appears a solid solution phase having a considerable excess of MnO over the stoichiometric representation. At 1300°C the manganese chromite solid solution field extends from $N_{\text{MnO}} = 0.500$ to $N_{\text{MnO}} = 0.595$.

TABLE VI : Phases present in the samples along the
MnO - Cr₂O₃ join. (T = 1300°C , P_{O₂} = 10^{-8.18} atm.)

Sample No.	Sample Composition (mole fraction)		Phases Present after Equilibration.
	N _{MnO}	N _{Cr₂O₃}	
36	0.45	0.45	Manganese chromite + Cr ₂ O ₃ ^g
37	0.48	0.48	Manganese chromite + Cr ₂ O ₃ ^e
38	0.50	0.50	Manganese chromite
39	0.55	0.45	Manganese chromite
40	0.59	0.41	Manganese chromite
41	0.60	0.40	Manganese chromite + MnO

4.5. The Spinel + Oxide Phase Boundary

The results presented the previous two sections show that spinel solid solutions should have a stability field within the MnO-NiO-Cr₂O₃ ternary so that a boundary line should exist to delineate the separation of chromite and oxide solid solutions. In Figure 12 this boundary is shown by the dashed lines extending from $N_{\text{MnO}}=0.595$ on the MnO-Cr₂O₃ join to $N_{\text{NiO}}=0.530$ on the NiO-Cr₂O₃ join. There are four additional points within the ternary field which help to define the location of this boundary. These points are indicated in Figure 12 and they are tabulated among data which will be presented in Section 4.6.2.

4.6. NiO Activities within the MnO-NiO-Cr₂O₃ Ternary

Twenty eight samples, compositions of which are marked in Figure 12, were selected within the ternary field for the measurement of NiO activities. For various phase fields shown in Figure 12 the following procedure was adopted in determining NiO activities.

4.6.1. NiO Activities in the Spinel + Cr₂O₃ Field

Samples marked from (1) to (5) are within this two phase field. These samples were equilibrated with gas atmospheres of continuously decreasing P_{O_2} until the

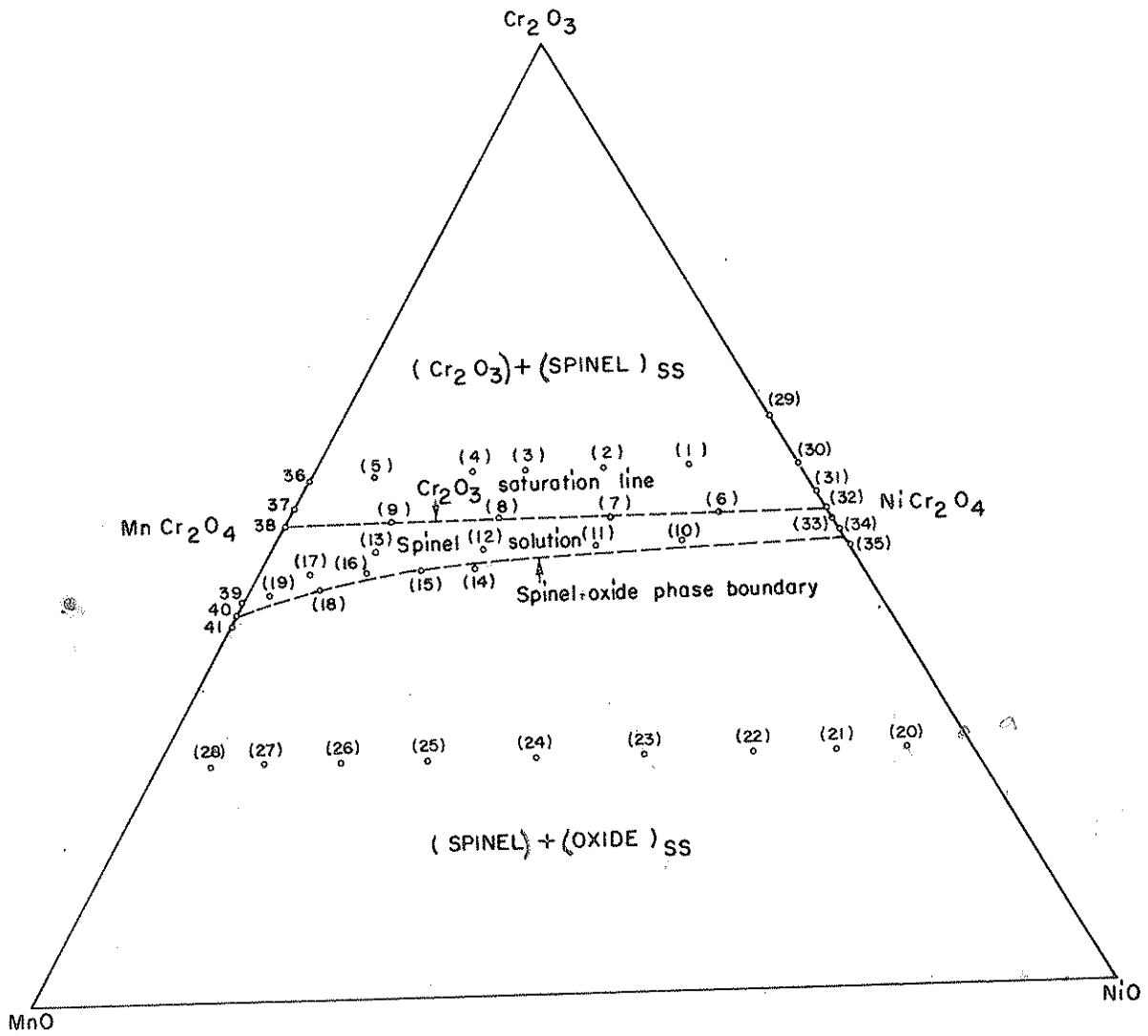


Figure 12 : The stability field of spinel solid solutions at 1300°C. The numbers in brackets represent the samples selected for NiO activity determinations.

precipitation of metallic nickel is observed on polished sections of the samples under microscope. The data on P_{O_2} are given in Table VII.

4.6.2. NiO Activities in the Spinel Field

Samples (6) to (19) are within this field. Sample number (14) happens to lie slightly outside the phase boundary while samples (15) and (18) are estimated to be on the phase boundary. The method of NiO activity determination in all these samples was the same as described in Section 4.6.1. The pertinent data are summarized in Table VII.

4.6.3. NiO Activities in the Spinel + Oxide Field

The samples numbered from (20) to (28) are within this field. The NiO activities of these samples were obtained, mainly, by determining the conjugation lines passing through them. A conjugation line, or a tie-line, is the line which connects the compositions of equilibrium phases. The conjugate phases which are located at the terminals of a conjugation line share the same thermodynamic properties.

In order to determine the directions of conjugation lines passing from samples (20) through (28), these samples were equilibrated at 1300°C for 12 hours each with gas atmospheres having partial pressures of oxygen slightly

TABLE VII : Data obtained in quenching experiments in the system
MnO - NiO - Cr₂O₃

Sample No.	Sample Composition (mole fraction)			Measured	Equilibrium	Present	Nickel Oxide
	N _{MnO}	N _{NiO}	N _{Cr₂O₃}	-log P _{O₂}	-log P _{O₂}	Phases	Activity
1.	0.10	0.35	0.55	7.9321		SS	
				7.9700		SS + Ni	
				8.0507		SS + Ni	
					7.9508		0.230 ± 0.001
2.	0.18	0.27	0.55	7.9509		SS	
				7.9700		SS	
				8.1167		SS + Ni (trace)	
				8.1543		SS + Ni	
				8.1167			0.190 ± 0.001
3.	0.25	0.20	0.55	7.9937		SS	
				8.0940		SS	
				8.1882		SS	
				8.2393		SS + Ni	
				8.2812		SS + Ni	
				8.2143			0.170 ± 0.001
4.	0.30	0.15	0.55	8.0984		SS	
				8.1680		SS	
				8.2436		SS	
				8.3758		SS	
				8.5604		SS + Ni	
				8.4735			0.126 ± 0.001

TABLE VII : (continued)

Sample No.	Sample Composition (mole fraction)			Measured	Equilibrium	Present	Nickel Oxide
	N_{MnO}	N_{NiO}	$N_{\text{Cr}_2\text{O}_3}$	$-\log P_{\text{O}_2}$	$-\log P_{\text{O}_2}$	Phases	Activity
5.	0.39	0.06	0.55	8.6785		SS	
				8.8197		SS	
				8.8724		SS	
				9.0135		SS	
				9.1165		SS	
				9.1789		SS + Ni	
				9.1179			0.060 ± 0.000
6.	0.10	0.40	0.50	7.9180		SS	
				8.0507		SS + Ni	
				7.9470			0.231 ± 0.001
7.	0.20	0.30	0.50	7.9223		SS	
				8.0333		SS	
				8.1118		SS + Ni (trace)	
				8.1874		SS + Ni	
				8.2572		SS + Ni	
				8.1161			0.191 ± 0.001
8.	0.30	0.20	0.50	8.3515		SS + Ni (trace)	
				8.3855		SS + Ni	
				8.3515			0.145 ± 0.001
9.	0.40	0.10	0.50	8.3954		SS	
				8.5015		SS	
				8.6499		SS	
				8.6967		SS	
				8.7425		SS	
				8.8197		SS	
				8.8722		SS + Ni (trace)	
				8.9876		SS + Ni	
				8.8722			0.080 ± 0.000

TABLE VII : (continued)

Sample No.	Sample Composition (mole fraction)			Measured	Equilibrium	Present	Nickel Oxide
	N_{MnO}	N_{NiO}	$N_{\text{Cr}_2\text{O}_3}$	$-\log P_{\text{O}_2}$	$-\log P_{\text{O}_2}$	Phases	Activity
10.	0.15	0.38	0.47	6.7188	6.7188	SS + Ni (trace)	0.950 ± 0.005
				6.7369		SS + Ni	
11.	0.23	0.30	0.47	6.8765	6.8987	SS	0.772 ± 0.004
				6.8900		SS	
				6.9077		SS + Ni	
				6.9452		SS + Ni	
12.	0.35	0.20	0.47	6.8146	7.0484	SS	0.650 ± 0.003
				6.8259		SS	
				6.9044		SS	
				6.9883		SS	
				7.0484		SS + Ni (trace)	
13.	0.43	0.10	0.47	8.1161	8.2328	SS	0.166 ± 0.001
				8.2163		SS	
				8.2496		SS + Ni	
				8.2745		SS + Ni	
14.	0.35	0.20	0.45	6.7032	6.7235	SS	0.945 ± 0.005
				6.7142		SS	
				6.7373		SS + Ni	
				6.7896		SS + Ni	
				6.8095		SS + Ni	

TABLE VII : (continued)

Sample No.	Sample Composition (mole fraction)			Measured	Equilibrium	Present	Nickel Oxide
	N _{MnO}	N _{NiO}	N _{Cr₂O₃}	-log P _{O₂}	-log P _{O₂}	Phases	Activity
15.	0.40	0.15	0.45	6.7416	6.7902	SS	0.875 ± 0.004
				6.7510		SS	
				6.7853		SS	
				6.8083		SS + Ni	
16.	0.45	0.10	0.45	7.5861	7.6113	SS	0.340 ± 0.002
				7.6372		SS + Ni	
17.	0.53	0.02	0.45	8.1925	8.3819	SS	0.140 ± 0.001
				8.2769		SS	
				8.5150		SS + Ni	
				8.5647		SS + Ni	
18.	0.50	0.07	0.43	6.7605	7.1107	SS	0.605 ± 0.003
				6.8248		SS	
				6.8509		SS	
				6.9169		SS	
				7.0716		SS	
				7.1036		SS	
				7.1267		SS + Ni	
19.	0.55	0.02	0.43	7.2056	7.4911	SS	0.390 ± 0.002
				7.2806		SS	
				7.4321		SS	
				7.4833		SS	
				7.4966		SS + Ni	

TABLE VII : (continued)

Sample No.	Sample Composition (mole fraction)			Measured	Equilibrium	Present	Nickel Oxide
	N_{MnO}	N_{NiO}	$N_{\text{Cr}_2\text{O}_3}$	$-\log P_{\text{O}_2}$	$-\log P_{\text{O}_2}$	Phases	Activity
25.	0.50	0.25	0.25	7.0893	7.1178	SS	0.600 ± 0.003
				7.1178		SS + Ni (trace)	
26.	0.58	0.17	0.25	7.3172	7.3430	SS	0.463 ± 0.002
				7.3700		SS + Ni	
27.	0.65	0.10	0.25	7.6424	7.6831	SS	0.313 ± 0.002
				7.7228		SS + Ni	

higher than that required for Ni precipitation. After equilibration, the samples were quenched, dried, and powdered for x-ray diffraction work. In x-ray analyses, the location of d_{200} peaks of oxide solid solutions were determined by using Cu-K α radiation at a scanning speed of $1^\circ/8$ min. d_{200} peaks correspond to reflections from (200) crystallographic planes, such peaks have the highest intensities compared to reflections from other planes.

The variation of the interplanar spacing d_{200} with the composition of MnO-NiO solid solutions has been measured by Hahn and Muan⁹; the graph illustrating this relationship is shown in Figure 13. Hence, by comparing the d_{200} values obtained from x-ray analysis of the present study with the graph shown in Figure 13 it has been possible to determine the compositions of the (Mn,Ni)O solid solutions present in two phase samples. A straight line passing through the sample and the composition of the oxide solid solution on the MnO-NiO join gives the direction of the conjugation line for that sample. In Table VIII the values of 2θ measured for (200) peaks, the corresponding d_{200} spacings, and the compositions of the conjugate oxide solid solutions as read from Figure 13 are given for samples belonging to the Spinel + Oxide field. The last column of this table shows a_{NiO} and a_{MnO} values obtained by inserting the oxide compositions in Figure 10. Because, conjugate phases have the same thermodynamic properties, the activities of NiO and MnO at the points where the conjugation lines

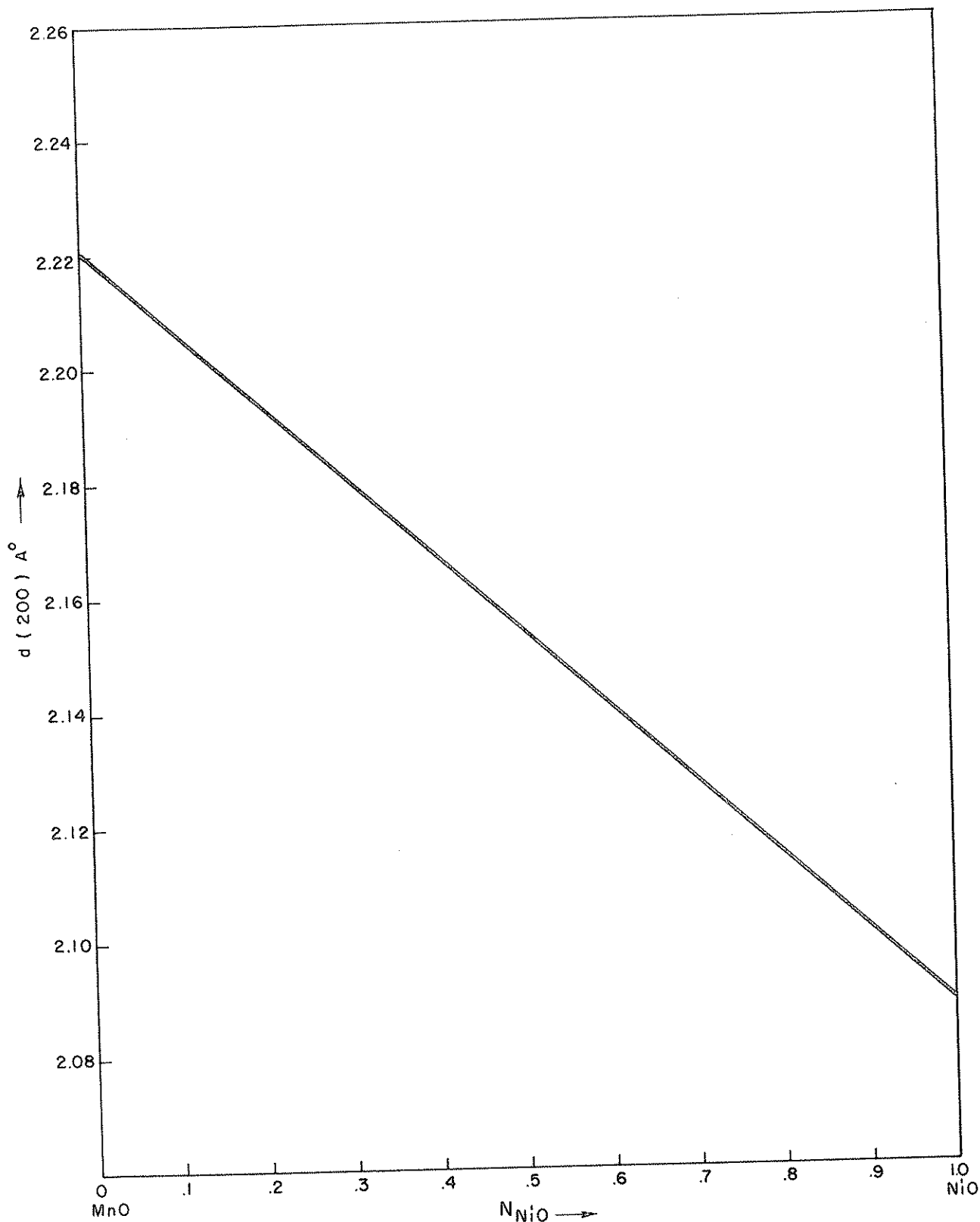


Figure 13 : Changes in d - spacing with composition in the system MnO - NiO. After Hahn and Muan⁹.

Table VIII : d_{200} as a function of composition in the system
 $\text{MnO} - \text{NiO} - \text{Cr}_2\text{O}_3$, and activities of NiO and MnO.

Samp. No.	Sample Composition (mole fraction)			2θ	$d_{(200)}^{\text{A}^\circ}$	Composition* of the conjugate oxide phase N_{NiO}	Activities**	
	N_{MnO}	N_{NiO}	$N_{\text{Cr}_2\text{O}_3}$				a_{NiO}	a_{MnO}
20	0.06	0.69	0.25	43.319	2.0889	0.990	0.990	0.012
21	0.125	0.625	0.25	43.317	2.0890	0.976	0.980	0.033
22	0.20	0.55	0.25	43.174	2.0956	0.946	0.950	0.054
23	0.30	0.45	0.25	42.983	2.1045	0.825	0.850	0.260
24	0.40	0.35	0.25	42.638	2.1207	0.675	0.713	0.433
25	0.50	0.25	0.25	42.214	2.1410	0.505	0.590	0.590
26	0.58	0.17	0.25	41.660	2.1682	0.350	0.463	0.692
27	0.65	0.10	0.25	41.200	2.1913	0.200	0.307	0.814
28	0.70	0.05	0.25	40.880	2.2077	0.098	0.170	0.904

(*) From Figure 13

(**) From Figure 10

meet the Spinel + Oxide phase boundary are those listed in Table VII. The activities of NiO in samples (25), (26), and (27) were determined also by nickel precipitation experiments, the values of P_{O_2} are listed in Table VII. Both the d_{200} -spacing measurements and direct activity determination yield nearly identical values for a_{NiO} in these samples.

4.7. Other Thermodynamic Calculations

From the data presented in the previous sections on NiO activities within the system MnO-NiO-Cr₂O₃ at 1300°C calculations can be made to gain information on the thermodynamic properties of spinel solid solutions at this temperature. In the following, first, the NiO data will be summarized graphically, and then we will proceed to calculate activities of other components of interest.

4.7.1. Graphical Representation of NiO Activities

The activities of NiO given in Tables IV, VII, and VIII are shown in the form of isoactivity curves for NiO in Figure 14. Within a two phase field, like Spinel + Oxide or Spinel + Cr₂O₃, an iso-activity curve assumes the form of a straight line owing to the fact that in such fields there is only one degree of freedom at the constant temperature of 1300°C.

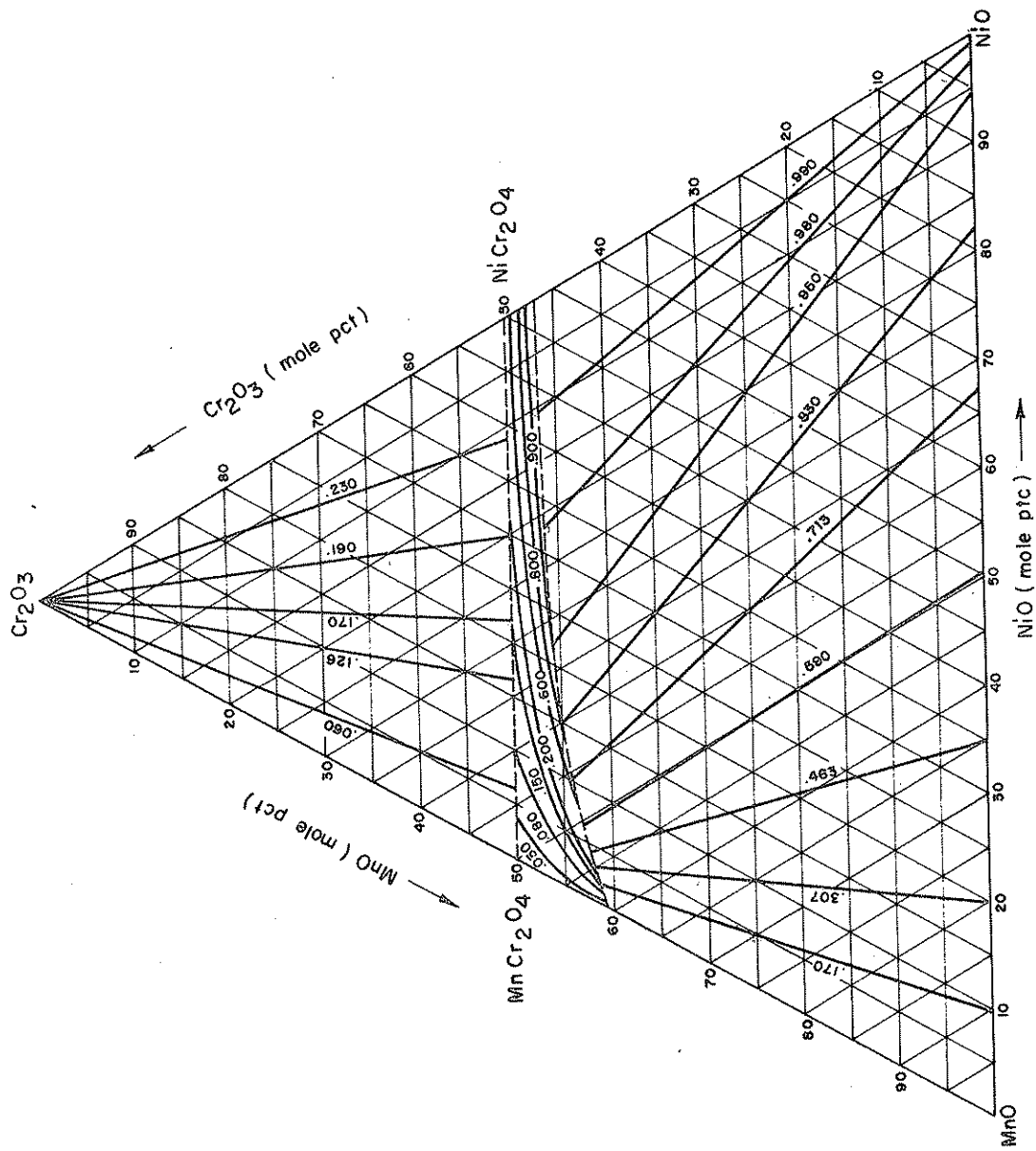


Figure 14 : Activities of NiO in the system MnO - NiO - Cr₂O₃ at 1300°C.

4.7.2. Activities of MnO and Cr₂O₃ in the Spinel Field

The activities of MnO and Cr₂O₃ in spinel solid solutions can be calculated by ternary Gibbs-Duhem integration of the measured NiO activities.

According to the method suggested by Schuhmann²¹, when the activities of component 1 in a ternary 1-2-3 systems are determined experimentally, the activities of, for example, component 2 can be obtained from the equation:

$$\log a_2^{\text{II}} = \left[\log a_2^{\text{I}} - \int_{\log a_1^{\text{I}}}^{\log a_1^{\text{II}}} \left(\frac{\partial n_1}{\partial n_2} \right)_{a_1, n_2} d \log a_1 \right]_{n_2/n_3} \quad (33)$$

In Equation (33), n_2/n_3 indicates that the integration should be performed along paths of constant n_2/n_3 ratio. Such paths are straight lines originating from the apex 1 of the composition triangle and terminating at the 2-3 side of it. The term $(\partial n_1 / \partial n_2)_{a_1, n_2}$ is called the "tangent-intercept" term. In order to obtain $(\partial n_1 / \partial n_2)$ at each known a_1 , the procedure outlined in the schematic drawings of Figure 15 is followed. In short, this procedure consists of drawing tangent to the iso-activity curves of component 1 at the points where the integration path n_2/n_3 cuts these curves. The intercept of a tangent on the 1-2 side of the triangle converted to the mole fraction ratio n_1/n_2 gives the value of the tangent-intercept $(\partial n_1 / \partial n_2)$ at the particular a_1 value.

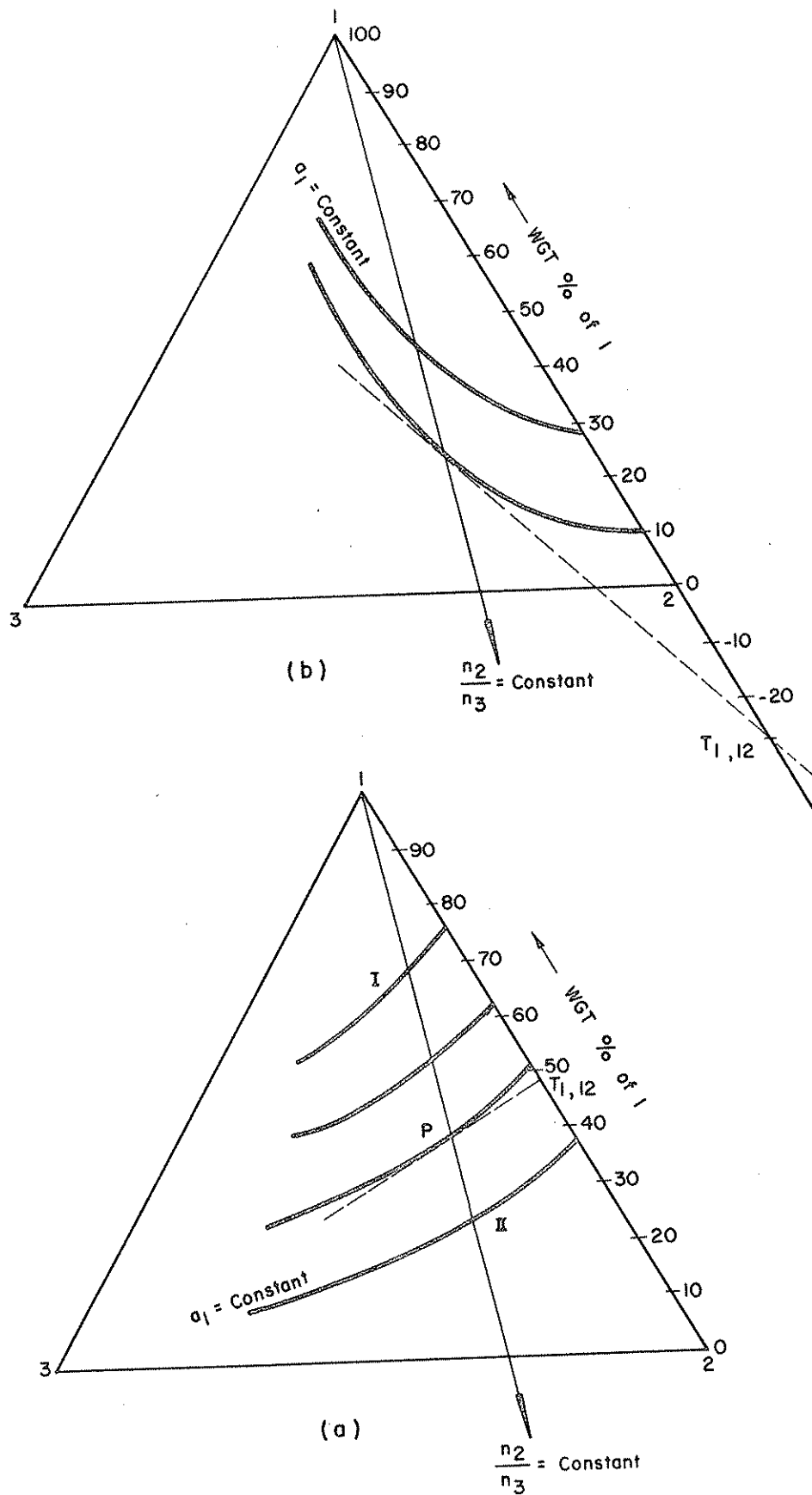


Figure 15 : Ternary isotherm showing the construction of (a) positive tangent - intercepts, and (b) negative tangent - intercepts ($T_{1,12}$).

The integral on the right-hand-side of Equation (33) is evaluated graphically by measuring the area under the $(\partial n_1 / \partial n_2)$ versus $\log a_1$ curve between the points $\log a_1^I$ and $\log a_1^{II}$. For complete evaluation of Equation (33) along any integration path n_2/n_3 , the value of $\log a_2^I$ must be known at the starting point of integration.

For the activities of Cr_2O_3 and MnO , Equation (33) can be written as:

$$\log a_{\text{Cr}_2\text{O}_3}^{II} = \left[\log a_{\text{Cr}_2\text{O}_3}^I - \int_{\log a_{\text{NiO}}^I}^{\log a_{\text{NiO}}^{II}} \left(\frac{\partial n_{\text{NiO}}}{\partial n_{\text{Cr}_2\text{O}_3}} \right) a_{\text{NiO}, n_{\text{Cr}_2\text{O}_3}} \cdot d \log a_{\text{NiO}} \right] \cdot n_{\text{Cr}_2\text{O}_3 / n_{\text{MnO}}} \quad (34)$$

$$\log a_{\text{MnO}}^{II} = \left[\log a_{\text{MnO}}^I - \int_{\log a_{\text{NiO}}^I}^{\log a_{\text{NiO}}^{II}} \left(\frac{\partial n_{\text{NiO}}}{\partial n_{\text{MnO}}} \right) a_{\text{NiO}, n_{\text{MnO}}} \cdot d \log a_{\text{NiO}} \right] \cdot n_{\text{MnO} / n_{\text{Cr}_2\text{O}_3}} \quad (35)$$

In order to obtain Cr_2O_3 activities within the spinel field Equation (34) was evaluated along several constant $n_{\text{Cr}_2\text{O}_3} / n_{\text{MnO}}$ paths. The starting values of $\log a_{\text{Cr}_2\text{O}_3}^I$ are taken along the NiCr_2O_4 - MnCr_2O_4 join where $a_{\text{Cr}_2\text{O}_3}^I = 1$, since this join represents the Cr_2O_3 saturation boundary.

For MnO activities Equation (35) was evaluated along the same path chosen for Equation (34), the starting $\log a_{\text{MnO}}^I$ values at each integration path was taken from

the Spinel + Oxide phase boundary, since a_{MnO} values are known along this boundary from the conjugation lines between spinel and oxide solid solutions.

The activities calculated from Equation (34) and (35) could be cross-checked by another equation obtained directly from the starting Gibbs-Duhem Equation of the following form:

$$n_{\text{NiO}} \cdot d \log a_{\text{NiO}} + n_{\text{MnO}} \cdot d \log a_{\text{MnO}} + n_{\text{Cr}_2\text{O}_3} \cdot d \log a_{\text{Cr}_2\text{O}_3} = 0 \quad (36)$$

If, for example, we consider a constant a_{NiO} path, then:

$$n_{\text{MnO}} \cdot d \log a_{\text{MnO}} + n_{\text{Cr}_2\text{O}_3} \cdot d \log a_{\text{Cr}_2\text{O}_3} = 0 \quad (37)$$

is obtained. Hence, the activity of MnO can be written as:

$$d \log a_{\text{MnO}} = - \frac{n_{\text{Cr}_2\text{O}_3}}{n_{\text{MnO}}} \cdot d \log a_{\text{Cr}_2\text{O}_3} \quad (38)$$

Equation (38) permits an easier route to arrive the MnO activities once those of Cr_2O_3 are evaluated by Equation (34).

The results of the Gibbs-Duhem calculations for the components MnO and Cr_2O_3 are given in Appendix II. MnO and Cr_2O_3 activities are shown in the form of iso-activity curves in Figure 16.

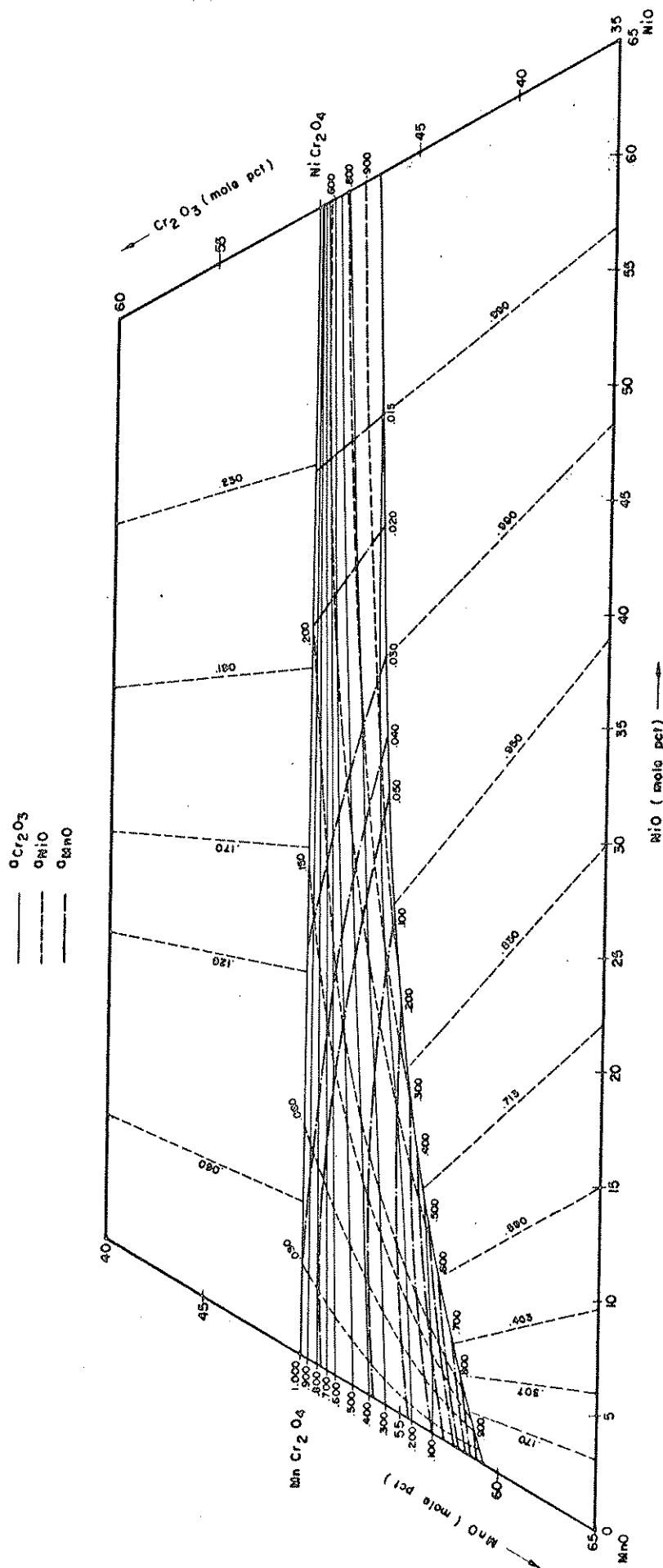


Figure 16: Activities of MnO, NiO and Cr₂O₃ in the system MnO-NiO-Cr₂O₃ at the temperature 1300°C.

4.7.3. Activities of MnO and Cr₂O₃ in Manganese Chromite Solutions

The MnO activities calculated in the spinel solid solution field were extrapolated to the join MnO-Cr₂O₃ in order to estimate the MnO activities in manganese chromite solutions. The same could be done with Cr₂O₃ activities, but, the accuracy of Cr₂O₃ activities decreases when we approach MnO-Cr₂O₃ side because integrations by Equation (34) become impossible since $\log a_{\text{Cr}_2\text{O}_3}^{\text{I}}$ values are unknown along integration path having $n_{\text{MnO}}/n_{\text{Cr}_2\text{O}_3} > 1$.

The MnO activities in Manganese chromite solutions obtained by extrapolating the iso-MnO activity curves within the spinel field are given in Table IX. From MnO activities, the activities of Cr₂O₃ in chromite solutions are calculated by a binary Gibbs-Duhem integration. The results are shown in the last column of Table IX. Figure 17 displays the MnO and Cr₂O₃ activities of manganese chromite solution as a function of composition.

4.7.4. Standard Free Energy of Formation of MnCr₂O₄

The formation of MnCr₂O₄ from MnO and Cr₂O₃ is expressed by the following reaction:



TABLE IX : Activities of Cr_2O_3 in the $\text{MnO} - \text{Cr}_2\text{O}_3$ system at 1300°C

Sample Composition (mole fraction)		a_{MnO}	$\frac{n_{\text{MnO}}}{n_{\text{Cr}_2\text{O}_3}}$	$-\log a_{\text{Cr}_2\text{O}_3}$	$a_{\text{Cr}_2\text{O}_3}$
N_{MnO}	$N_{\text{Cr}_2\text{O}_3}$				
0.50	0.500	0.042	1.000	0	1.000
0.517	0.483	0.068	1.070	0.219	0.604
0.533	0.467	0.088	1.141	0.343	0.454
0.545	0.455	0.161	1.215	0.651	0.223
0.565	0.435	0.320	1.315	1.029	0.094
0.595	0.405	1.000	1.439	1.712	0.020

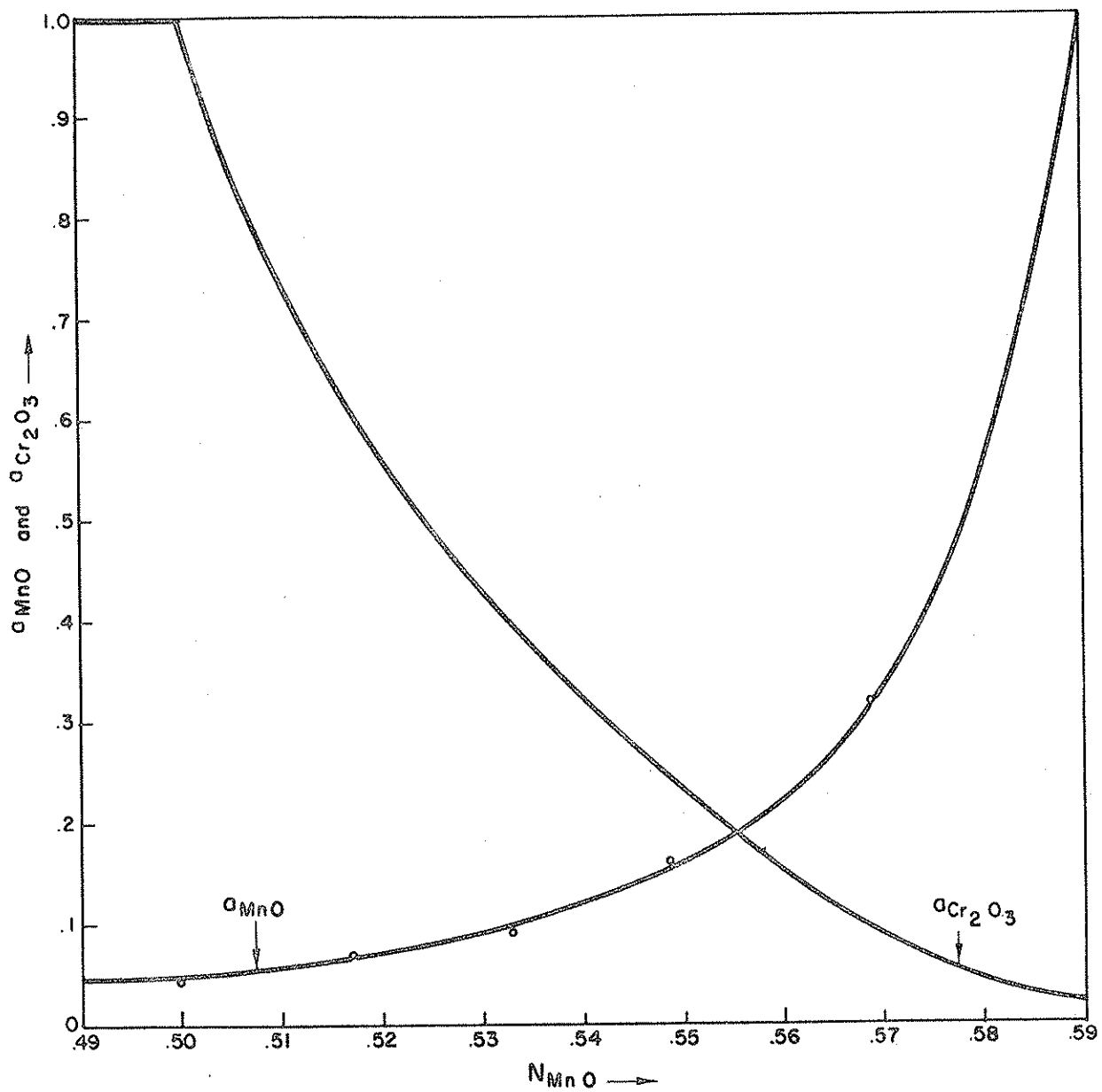


Figure 17 : Activity - composition relations in the MnO - Cr₂O₃ system.

The standard free energy change of Reaction (39) is given by:

$$\Delta G^{\circ} = -RT \ln \frac{a_{\text{MnCr}_2\text{O}_4}}{a_{\text{MnO}} \cdot a_{\text{Cr}_2\text{O}_3}} \quad (40)$$

At the stoichiometric MnCr_2O_4 composition, $a_{\text{MnCr}_2\text{O}_4} = 1$ and $a_{\text{Cr}_2\text{O}_3} = 1$; the value of a_{MnO} being 0.042 (Figure 17 and Table IX) at this point. Hence, from Equation (40) at 1300°C .

$$\Delta G^{\circ} = -41588 \text{ J/gfw.} \quad (41)$$

-41588 J/gfw represents the standard free energy of formation of MnCr_2O_4 from its component oxides MnO and Cr_2O_3 at 1300°C .

4.7.5. Activity-Composition relations in MnCr_2O_4 - NiCr_2O_4 Solid Solutions.

Along the join MnCr_2O_4 - NiCr_2O_4 there exist the stoichiometric chromite solid solutions. The activities of NiCr_2O_4 in these solutions at 1300°C can be calculated from Equation(31) which can be rearranged to the form:

$$a_{\text{NiCr}_2\text{O}_4} = \frac{a_{\text{NiO}}}{0.255} \quad (42)$$

where a_{NiO} happens to represent the nickel oxide activities on the MnCr_2O_4 - NiCr_2O_4 join and are shown in Figure 18.

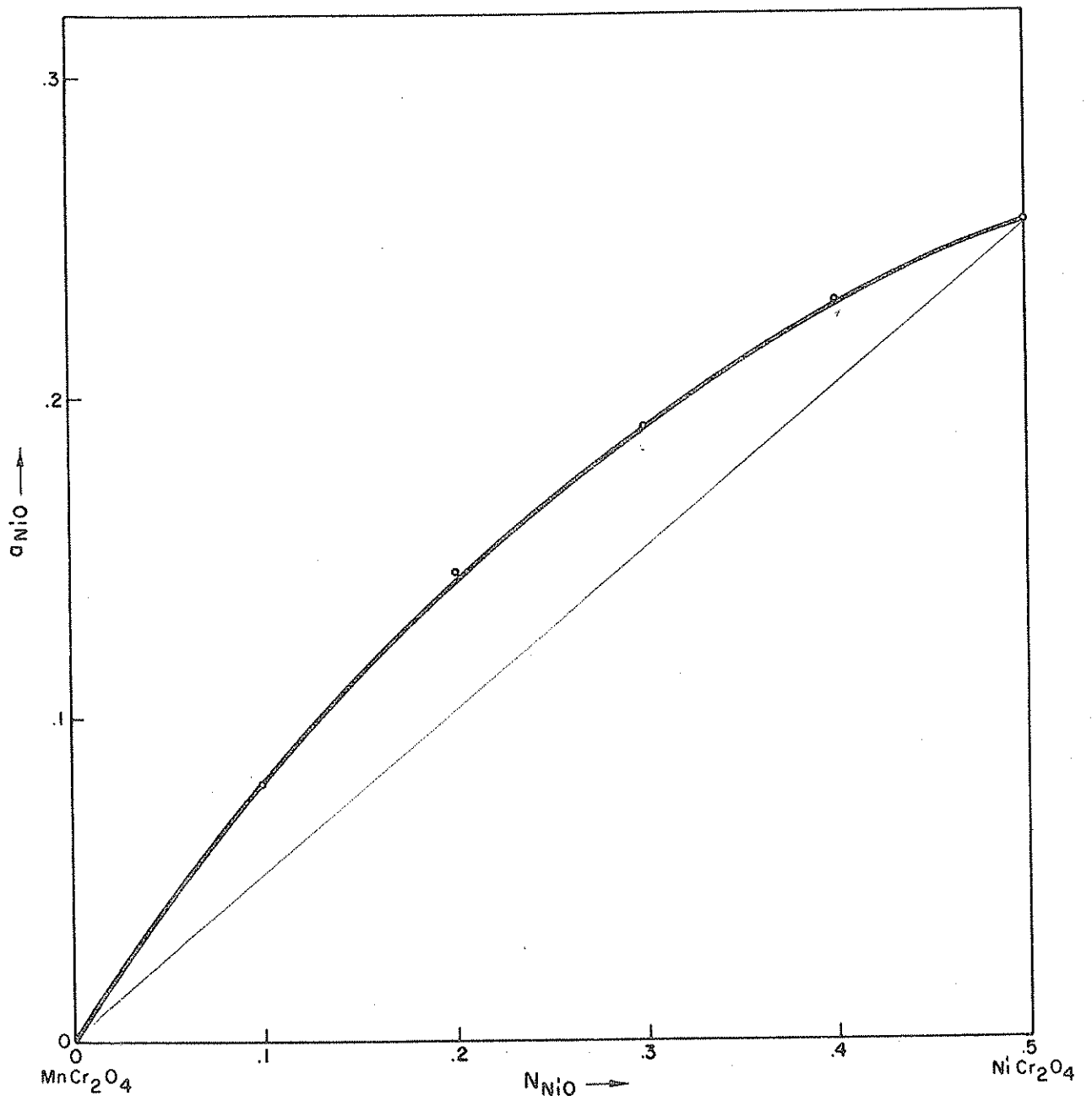


Figure 18: NiO activities along the join $MnCr_2O_4 - NiCr_2O_4$.

The NiCr_2O_4 activities obtained from Equation (42) are given in Table X. The activities of MnCr_2O_4 are calculated from the Gibbs-Duhem treatment of NiCr_2O_4 activities by using the expression:

$$\ln \gamma_{\text{MnCr}_2\text{O}_4} = -N_{\text{MnCr}_2\text{O}_4} \cdot N_{\text{MnCr}_2\text{O}_4} \cdot \alpha_{\text{NiCr}_2\text{O}_4} - \int_{N_{\text{MnCr}_2\text{O}_4}=1}^{N_{\text{MnCr}_2\text{O}_4}} \alpha_{\text{NiCr}_2\text{O}_4} \cdot dN_{\text{MnCr}_2\text{O}_4} \quad (43)$$

where $\alpha_{\text{NiCr}_2\text{O}_4}$ is defined by:

$$\alpha_{\text{NiCr}_2\text{O}_4} = \frac{\ln \gamma_{\text{NiCr}_2\text{O}_4}}{(N_{\text{MnCr}_2\text{O}_4})^2} \quad (44)$$

The results of the graphical integration of Equation (43) are given in the last column of Table X. Figure 19 displays the variation of chromite activities with composition. The chromite solutions exhibit slight positive departure from the ideal Raoultian behavior.

TABLE X : Activities of NiCr_2O_4 and MnCr_2O_4 as a function of composition in the $\text{MnCr}_2\text{O}_4 - \text{NiCr}_2\text{O}_4$ system.

Sample Composition (mole fraction)					
$N_{\text{NiCr}_2\text{O}_4}$	$N_{\text{MnCr}_2\text{O}_4}$	$N_{\text{Cr}_2\text{O}_3}$	a_{NiO}	$a_{\text{NiCr}_2\text{O}_4}$	$a_{\text{MnCr}_2\text{O}_4}$
1.0	0.0	0.50	0.255	1.000	0.000
0.9	0.1	0.50	0.245	0.9608	0.213
0.8	0.2	0.50	0.231	0.905	0.306
0.7	0.3	0.50	0.212	0.831	0.396
0.6	0.4	0.50	0.191	0.749	0.481
0.5	0.5	0.50	0.169	0.662	0.544
0.4	0.6	0.50	0.145	0.568	0.630
0.3	0.7	0.50	0.114	0.447	0.715
0.2	0.8	0.50	0.080	0.313	0.804
0.1	0.9	0.50	0.042	0.164	0.900
0.0	1.0	0.50	0.000	0.000	1.000

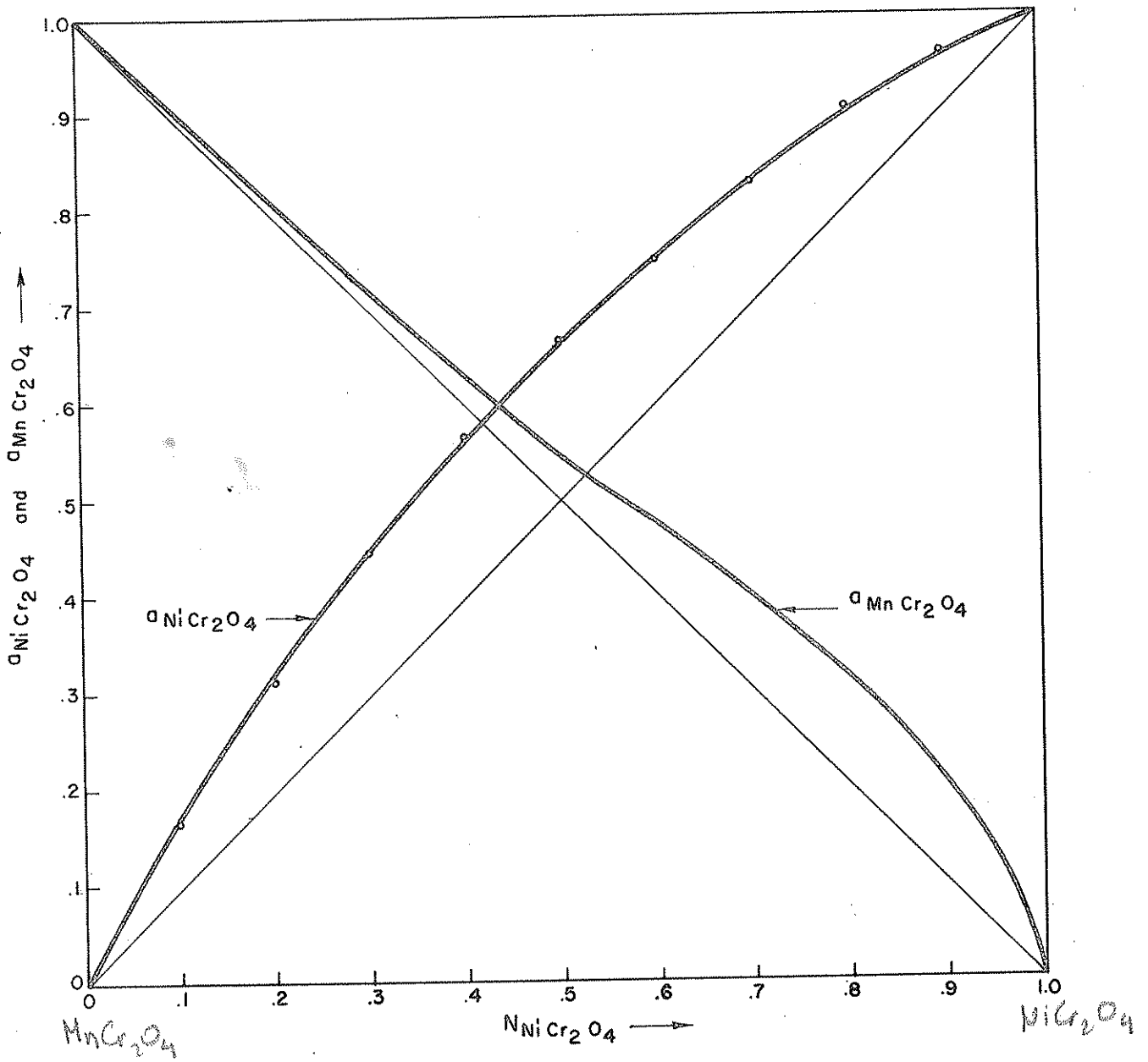


Figure 19 : Activities of NiCr_2O_4 and MnCr_2O_4 as a function of composition in the system $\text{MnCr}_2\text{O}_4 - \text{NiCr}_2\text{O}_4$.

CHAPTER V

DISCUSSION and CONCLUSIONS

The present work was concerned with the determination of equilibria and thermodynamics of MnO-NiO-Cr₂O₃ system at 1300°C. The system is characterized by two solid solution series; (a) MnO-NiO solutions, and (b) Chromite solutions. The experimental work involved determining the activities of NiO in both type of solutions by equilibrating samples belonging to them with a gas phase of known oxygen partial pressure. The accuracies of measured NiO activities, and hence the activities of other components derived by Gibbs-Duhem treatment of a_{NiO} data are affected mainly by the errors involved in P_{O_2} values. The $\log P_{\text{O}_2}$ values reported in various tables of this thesis are estimated to be correct to within ± 0.010 ; this estimate is based on the errors that could be made in reading the heights of the manometer liquids of the gas mixer. As explained in Section 4.2. nickel oxide activities were calculated from the expression:

$$a_{\text{NiO}} = \left(\frac{P_{\text{O}_2}}{P_{\text{O}_2}^*} \right)^{1/2} \quad (23)$$

Thus the error expression for a_{NiO} would be:

$$\Delta a_{\text{NiO}} = \frac{1}{2} a_{\text{NiO}} (\Delta \log P_{\text{O}_2}) \quad (45)$$

Equation (45) can be used to calculate errors involved in various values of a_{NiO} . A critical nickel oxide activity, for example, is 0.255, this value affects the standard free energy of formation of NiCr_2O_4 , and it also affects the activity-composition relations in MnCr_2O_4 - NiCr_2O_4 solutions. From Equation (45), the error in $a_{\text{NiO}} = 0.255$ can be calculated as follows:

$$\Delta a_{\text{NiO}} = \frac{1}{2} \times (0.255) \times (0.010) = 0.001$$

Hence the gas mixing system permits to measure low NiO activities with greater accuracy. The error reflected upon ΔG° of NiCr_2O_4 at 1300°C would be:

$$\begin{aligned} \Delta(\Delta G^\circ) &= \Delta(RT \log a_{\text{NiO}}). & (46) \\ &= RT \Delta(\log a_{\text{NiO}}) \\ &= RT \frac{\Delta a_{\text{NiO}}}{a_{\text{NiO}}} \\ &= \mp 120 \text{ J/gfw.} \end{aligned}$$

When the error in temperature is also taken into consideration, the error equation becomes:

$$\Delta(\Delta G^\circ) = R \left[\Delta T \cdot \log a_{\text{NiO}} + T \cdot \frac{\Delta a_{\text{NiO}}}{a_{\text{NiO}}} \right]. \quad (47)$$

In the present study, the temperatures were measured and controlled with an estimated accuracy of $\mp 2^\circ\text{C}$. At 1300°C

based on a maximum error of 2°C in temperature, error in ΔG° of NiCr_2O_4 will be:

$$\Delta(\Delta G^\circ) = \pm 140 \text{ J/gfw.}$$

Thus, according to the present results, the standard free energy of formation of the nickel chromite compound from its component oxides is $-17,484.8 \pm 140 \text{ J/gfw}$. This value is in fairly good agreement with that obtained from Equation (8) in Section 2.4. At 1300°C. Equation (8) yields $-20,085 \pm 400 \text{ J/gfw}$; other ΔG° equations predict grossly different results.

Apart from quantitative errors involved in the measurement of NiO activities mentioned above, an additional source of error is involved in the interpretation of metallographic specimens. If the starting pellets are inhomogeneous, the nickel precipitates appear as localized clusters as shown in the micro-photograph of Figure 20. In homogeneous samples, on the other hand, nickel precipitation occurs uniformly throughout the entire specimen section as shown in Figure 21. In this work, the samples showing clusters of nickel precipitates are discarded and new pellets were prepared in order to eliminate to uncertainties originating from inhomogeneous samples.

In the MnO-NiO system, the NiO activities determined in this work are in very good agreement with the gas equilibration results of Hahn and Muan⁹ and with the

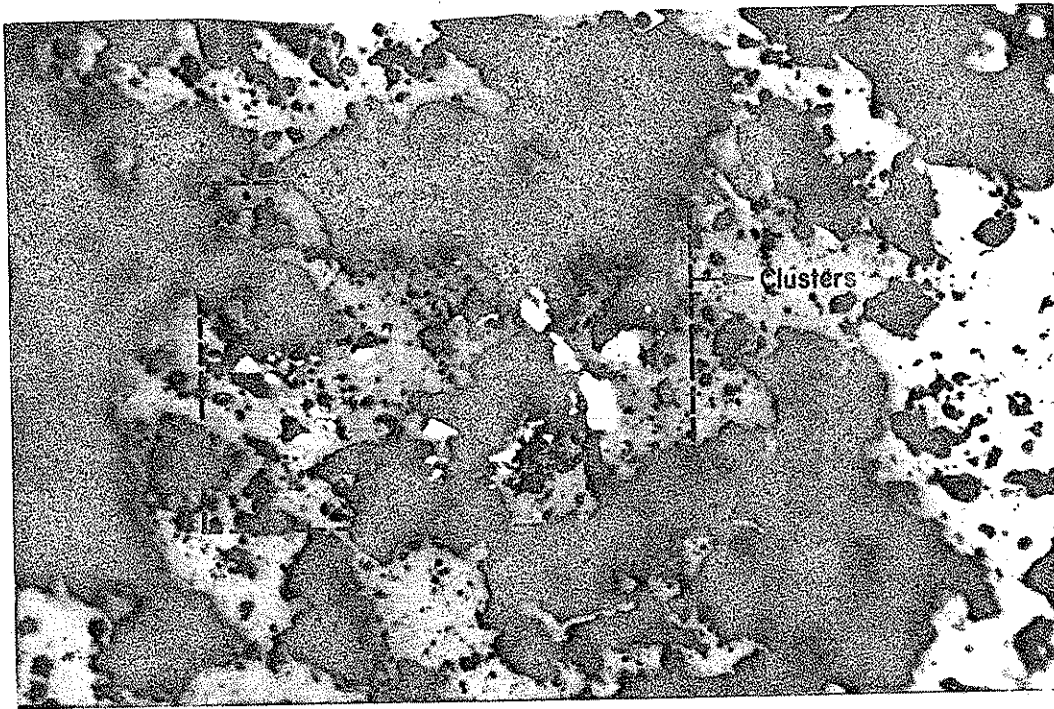


Figure 20 : The micro-photograph of the sample containing clusters of nickel precipitates.

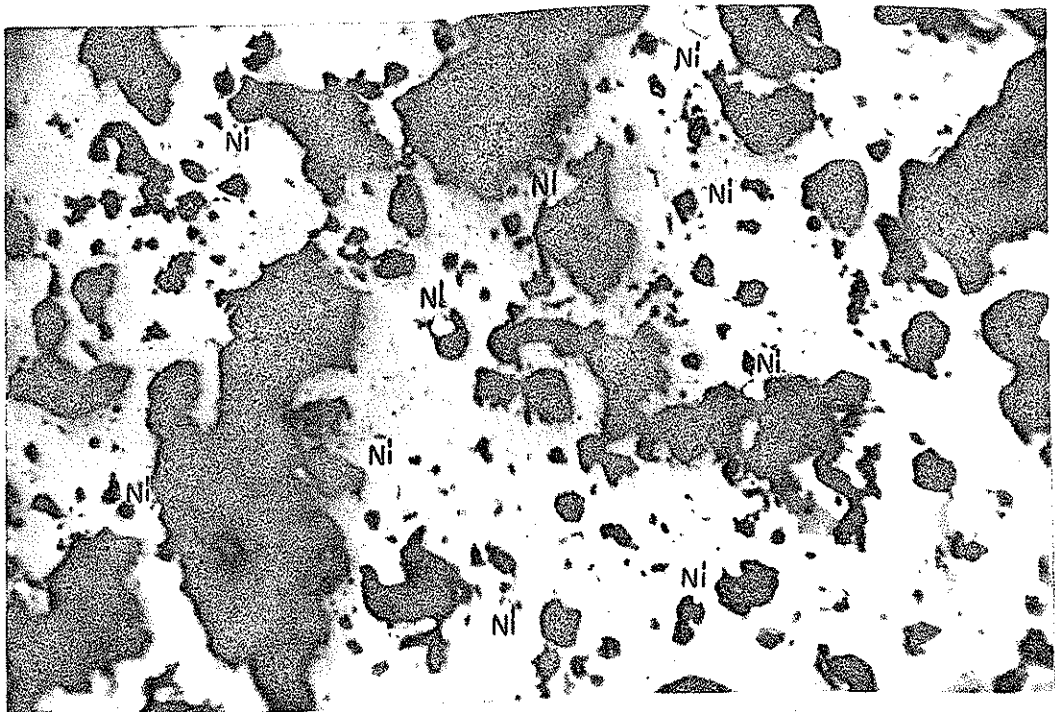


Figure 21 : The micro-photograph of the sample containing uniform nickel precipitates.

extrapolations to 1300°C of the emf data provided by Cameron and Unger¹⁴. This solid solution series exhibits a moderate positive departure from ideal behaviour.

The manganese chromite and nickel chromite came out as nonstoichiometric compounds, in both of these normal spinels the nonstoichiometry appears to be associated with the tetrahedral sites, because MnCr_2O_4 dissolves excess MnO, and NiCr_2O_4 dissolves excess NiO. As the results, the ternary (Mn-Ni) Cr_2O_4 solid solutions have a stability field a boundary of which is shared by the (Mn-Ni)O solid solutions. This new observation is in contrast to the conclusions of Jacob and Fitzner¹⁸ on the MnO-CoO- Cr_2O_3 system at 1100°C. They have inferred that, MnCr_2O_4 and CoCr_2O_4 do not dissolve any excess of MnO or CoO, but instead both compounds can take up a slight excess of Cr_2O_3 into their structures. Thus the Spinel+Oxide phase boundary becomes the MnCr_2O_4 - CoCr_2O_4 join in their work, and an estimated phase boundary is drawn¹⁸ to show the Cr_2O_3 saturation. As the result of the differences explained above the standard free energy of formation of MnCr_2O_4 calculated by Jacob and Fitzner¹⁸ at 1100°C is largely different than that obtained in this work at 1300°C. In contrast to the value -59065 J/gfw reported¹⁸ at 1100°C, this work predicted -41588 J/gfw for ΔG° of MnCr_2O_4 at 1300°C. In general the entropy terms in ΔG° of spinels are rather small¹⁸, hence the values measured at 1100°C and 1300°C should not have such gross differences.

When the ΔG° values of MnCr_2O_4 and NiCr_2O_4 obtained in this work are compared, MnCr_2O_4 appears to be much more stable than NiCr_2O_4 at 1300°C . This conclusion is supported by the directions of the conjugation lines between coexisting $(\text{Mn-Ni})\text{O}$ and $(\text{MnO-NiO})\text{Cr}_2\text{O}_3$ solid solutions, depicted in Figure 14. These lines are directed toward the MnCr_2O_4 composition point rather than the NiCr_2O_4 composition point, meaning that the manganese chromite should be more stable than nickel chromite. A further support of this conclusion lies in the oxidation studies of Lowell⁵, electron microprobe analysis⁵ showed that the spinel phase of the oxide scale forming on a manganese containing stainless steel was mainly MnCr_2O_4 . Truly, this spinel should be a solution, and it should be in equilibrium with a $(\text{Mn,Ni})\text{O}$ solid solution.

The activities of MnCr_2O_4 and NiCr_2O_4 in stoichiometric chromite solid solutions were observed to deviate positively from Raoultion behavior as shown Figure 19. The NiCr_2O_4 activity curve does not approach the Raoult law line with the expected slope at compositions approaching pure NiCr_2O_4 . This may be attributed either to inaccurate NiO activities measured around this composition, or the cause might lie in the position of the Cr_2O_3 saturation boundary. In the present work this boundary coincided with the MnCr_2O_4 - NiCr_2O_4 join, but if it goes as predicted by Jacob and Fitzner¹⁸ the shape of the NiCr_2O_4 activity curve may change to confirm with the Raoultion behavior at the NiCr_2O_4 side. Repeated activity measurements along the NiCr_2O_4 - Cr_2O_3

join of the system give consistent $a_{\text{NiO}} = 0.255$ values for all the samples studied along this join. Furthermore the iso-activity lines in the field Spinel + Cr_2O_3 met the MnCr_2O_4 - NiCr_2O_4 join at almost exactly the same NiO activities measured along this join. Hence, there was no evidence for passing the Cr_2O_3 saturation boundary above the MnCr_2O_4 - NiCr_2O_4 as suggested by Jacob and Fitzner¹⁸.

REFERENCES

1. C.S.Giggins and F.S.Petit: "Oxidation of Ni-Cr Alloys Between 800°C and 1200°C." Trans. TSM-AIME, 1969, vol. 245, pp. 2495-507.
2. C.S.Giggins and F.S.Petit: "The Effect of Grain-Size and Surface Deformation on the Selective Oxidation of Chromium in Ni-Cr Alloys at Temperatures of 900° and 1100°C." Trans. TMS-AIME, 1969 vol. 245, pp. 2509-514.
3. F.K.Aleinkov, V.A.Parfenow, G.Gabsyte, and R.Panlavicius: "High-Temperature stability of Combined Electrolytic Coatings. Nickel Coating with the Cr Particle Inclusions." Liet TSR Mokslu Akad Darb., Ser.B., 1973, (3), pp.69-79.
4. M.D.Merz: "The Oxidation Resistance of Fine-Grained Sputter-Deposited 304 Stainless Steel." Met. Trans. A, 1979, vol. 10A, pp. 71-77.
5. C.E.Lowell: "Cyclic and Isothermal Oxidation Behavior on Some Ni-Cr Alloys." Oxidation of Metals, 1973, vol. 7, pp. 95-115.
6. A.Muan and B.Phillips: "Equilibrium Relations in the System Manganese-Oxygen." Am. J. Sci., 1960, vol. 258, pp. 66-78.
7. C.E.Wicks and F.C.Block: "Thermodynamic Properties of 65 Elements, Their Oxides, Halides, Carbides, and Nitrides." U.S. Bureau of Mines Bull, 1963, No: 605.

8. D.P.Bogatski, Zhur Obshchei Khim., 1951, vol.9 pp. 21
9. W.C.Hahn, Jr and A Muan: "Activity Measurements in Oxide Solid Solutions: The Systems NiO-MgO and NiO-MnO in the Temperature Interval 1000^o-1300^oC." J.Phys.Chem. Solids, 1961, vol. 19, pp. 338-348.
10. Von.J.D. Tretjakow and H.Schmalzried: "Zur Thermodynamik von Spinell Phasen." Bur Bunsengen Phys. Chem., 1965, vol. 69, pp. 396.
11. Steele B.C.H. and Alcock C.B. "Electromotive Force Measurements in High-Temperature Systems." The Institution of Mining and Metallurgy 44 Portland Place, London, W.I., 1968, pp. 19-22.
12. Haydn Davies and W.W.Smeltzer: "Oxygen and Metal Activities of the Chromium-Nickel-Oxygen System Between 900^o and 1100^oC." J. Electrochem. Soc., 1974, vol. 121 (4), pp. 543-9.
13. S.Seethalaman and K.P.Abraham: "Activity Measurements in Nickel Oxide-Manganese Oxide Solid Solutions." Inst. Mining Met. Trans. Sect., 1968, vol. 77, pp. C209-C211.
14. D.J.Cameron and A.E.Unger: "The Measurement of the Thermodynamic Properties of NiO-MnO Solid Solutions by a Solid Electrolyte Cell Technique." Metallurgical Trans., 1971, vol. 1, pp. 2615-2621.

15. W.Kunmann, D.B.Rogers and A Word: "The use of CO-CO₂ Atmospheres for the Preparation and Free Energy Determinations of Several Oxide System." J. Phys. Chem. Solids, 1963. vol. 24, pp. 1535-1538.
16. V.A.Levitskii, T.N.Rezuthina, and V.G.Dneprova: "Measurements of the Electromotive Force of Galvanic Cells with a Solid Electrolyte at Temperature over 1100°C. Thermodynamic Properties of NiCr₂O₄." Electrokhimiya, 1965, vol. 1(8), pp. 933-40.
17. V.A.Lenev and I.A.Novakhatski: "Thermodynamic Properties of Co and Ni Chromites." Zh. Fiz. Khim., 1966, vol. 40(9), pp. 2030-5.
18. K.T.Jacob, K.Fitzner: "Ion-Exchange Equilibria Between (Mn,Co)O Solid Solution and (Mn,Co)Cr₂O₄ and (Mn,Co) Al₂O₄ Spinel Solid Solutions at 1100°C." Journal of Material Sci., 1977(12), pp.481-488.
19. O. Kubaschewski, E.L. Evans and C.B. Alcock: "Metallurgical Thermochemistry." Fourth Edition, Pergamon Press, 1967.
20. L.S.Darken and R.W. Gurry: "Physical Chemistry of Metals." McGraw-Hill Book Company, Inc., Tokyo, 1953, pp. 261-266.
21. R.Schuhmann Jr: "Application of Gibbs-Duhem Equations in Ternary Systems." Acta Met., 1955, vol. 3, pp. 219-26.

APPENDIX I

Calculation of Nickel Oxide Activity at 1300°C.

Activities of nickel oxide at the 1300°C are calculated by extrapolating data obtained at 900°, 1000°, 1100°, 1200°C¹⁴. Enthalpy changes of NiO with respect to temperature is expressed as;

$$\Delta \bar{H}_{\text{NiO}} = R \frac{d \ln a_{\text{NiO}}}{d\left(\frac{1}{T}\right)} \quad (48)$$

Upon rearranging Equation (48), we obtain:

$$d \ln a_{\text{NiO}} = \frac{\Delta \bar{H}_{\text{NiO}}}{R} d\left(\frac{1}{T}\right) \quad (49)$$

$\log a_{\text{NiO}}$ versus $\frac{1}{T}$ diagram is shown in Figure 22 and data about these is tabulated in Table XI. All lines on this diagram are straight lines and slope of these equal to the $\frac{\Delta \bar{H}_{\text{NiO}}}{2.3 R}$. $\Delta \bar{H}_{\text{NiO}}$ is calculated at 1300°C by using the slope of the line equations and is plotted against the N_{NiO} in Figure 23.

Activities of NiO are calculated by substituting $\Delta \bar{H}_{\text{NiO}}$ values which are obtained from Figure 23 into Equation (49). Results are given in Table XII.

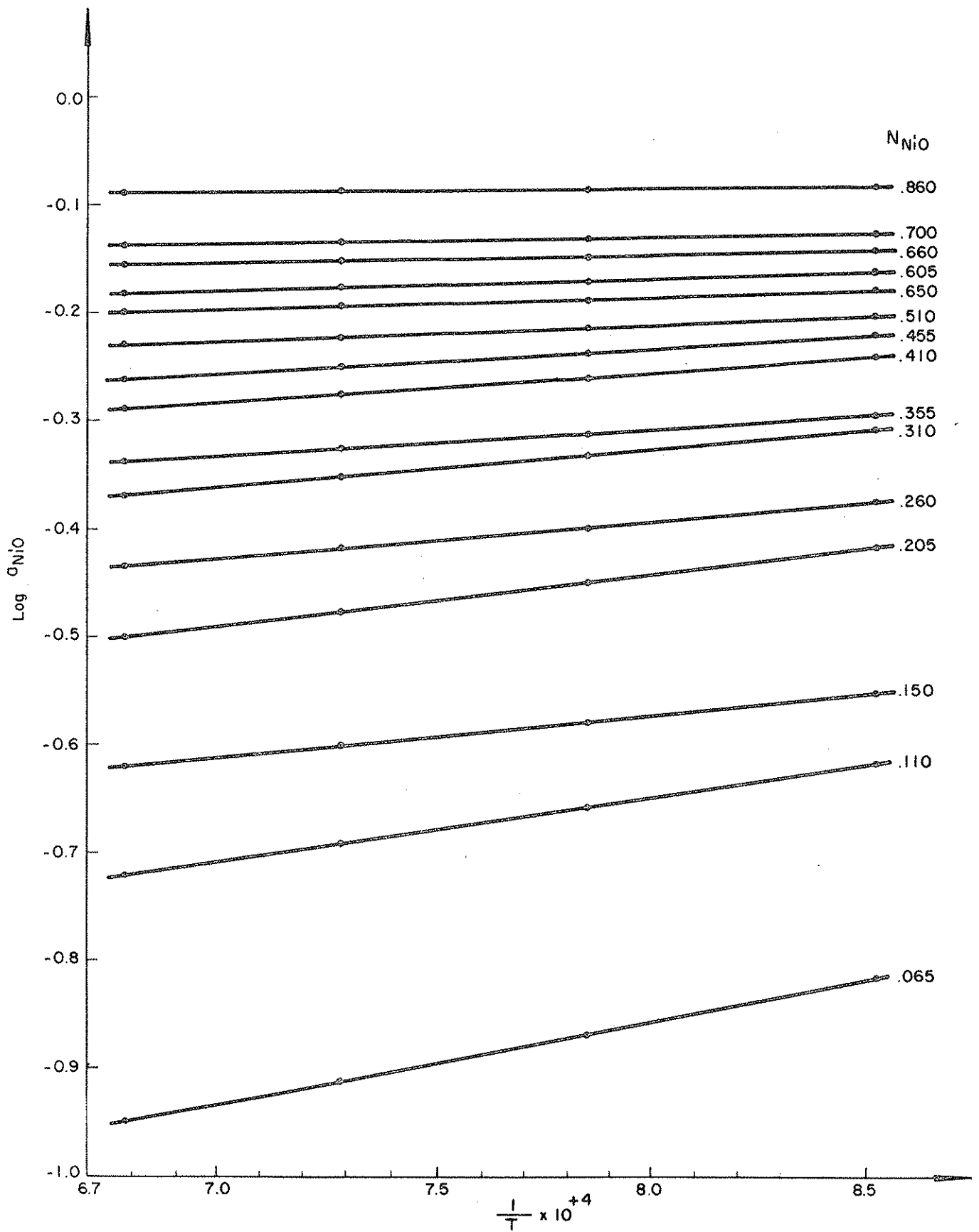


Figure 22 : $\log a_{NiO}$ versus $\frac{1}{T}$ diagram which is obtained by using the previous¹⁴ results.

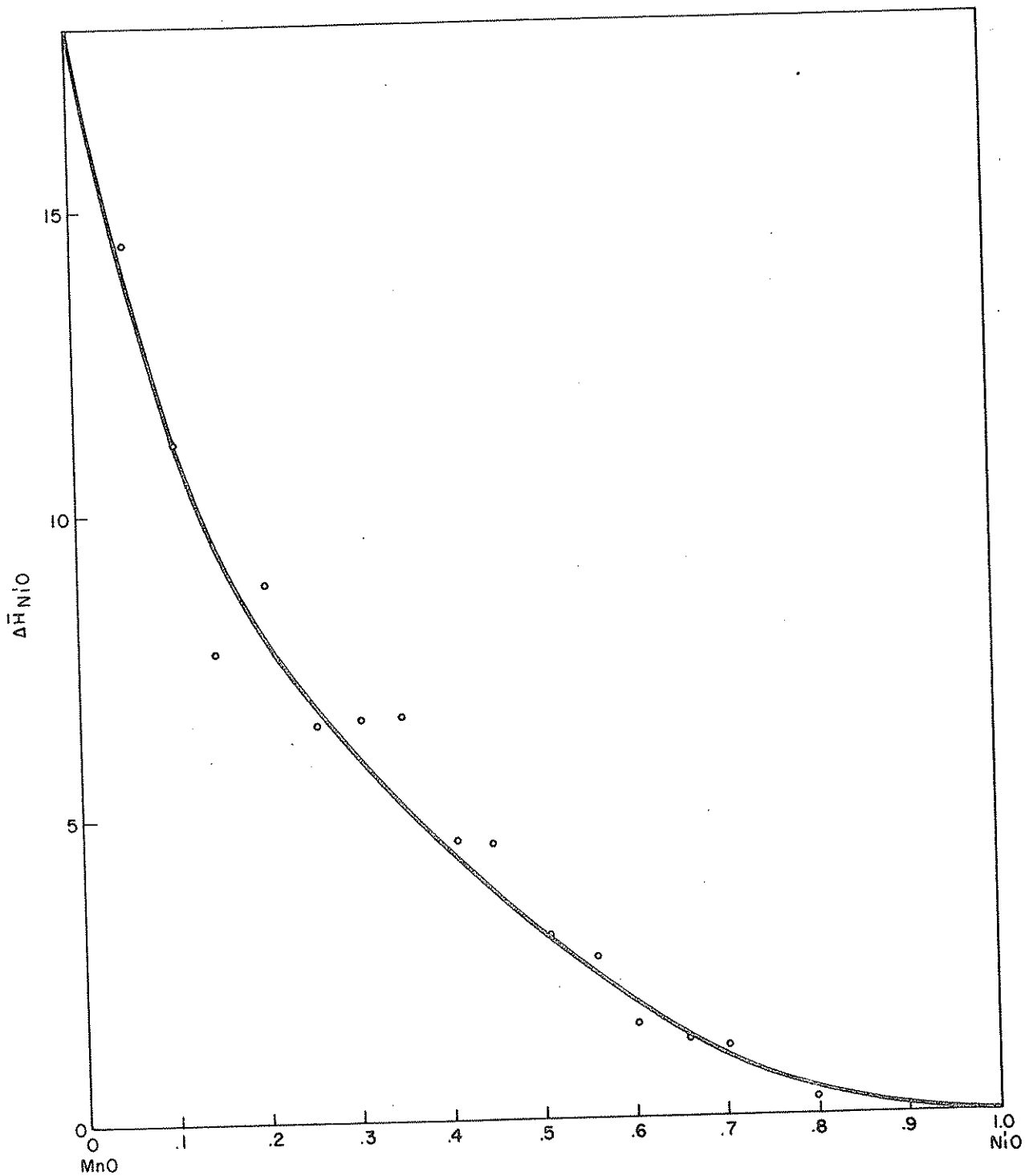


Figure 23 : $\Delta \bar{H}$ versus N_{NiO} diagram in NiO - MnO system. ✓

TABLE XI : $\log a_{\text{NiO}}$ as a function of composition in the MnO-NiO system at 900°, 1000°, 1100°, and 1200°C.


Sample Composition (mole fraction)		$-\log a_{\text{NiO}}$			
N_{NiO}	N_{MnO}	900°C	1000°C	1100°C	1200°C
0.065	0.935	0.815	0.870	0.910	0.947
0.110	0.890	0.620	0.659	0.692	0.721
0.150	0.850	0.550	0.580	0.600	0.620
0.205	0.795	0.419	0.448	0.475	0.499
0.260	0.740	0.375	0.400	0.418	0.434
0.310	0.690	0.308	0.333	0.353	0.367
0.410	0.590	0.244	0.261	0.273	0.286
0.455	0.545	0.220	0.237	0.250	0.261
0.510	0.490	0.203	0.215	0.223	0.230
0.560	0.440	0.176	0.186	0.194	0.200
0.605	0.395	0.166	0.173	0.177	0.180
0.660	0.340	0.143	0.148	0.151	0.154
0.705	0.295	0.127	0.131	0.134	0.137
0.800	0.200	0.086	0.088	0.088	0.089

TABLE XII : Activities of NiO as a function of composition at 1300°C

N_{NiO}	$-\log a_{\text{NiO}}(1200^{\circ}\text{C})$	$\Delta H(\text{J/degree mole})$	$-\log a_{\text{NiO}}(1300^{\circ}\text{C})$	$a_{\text{NiO}}(1300^{\circ}\text{C})$
0.065	.948	14450	.9806	.104
0.110	.720	11130	.745	.1798
0.150	.622	9500	.643	.227
0.205	.498	8050	.516	.305
0.260	.434	6720	.449	.356
0.310	.371	5800	.384	.413
0.410	.286	4250	.296	.506
0.455	.261	3700	.269	.538
0.510	.230	2950	.237	.580
0.560	.2007	2350	.206	.622
0.605	.1805	1820	.1846	.654
0.660	.1546	1300	.1575	.696
0.705	.1374	920	.1395	.725
0.800	.0894	400	.0903	.812

APPENDIX II. Activity calculations of Cr_2O_3 and MnO in
 $\text{MnO} - \text{NiO} - \text{Cr}_2\text{O}_3$ system at 1300°C .

TABLE XIII : Activity calculations of Cr_2O_3 in $\text{MnO} - \text{NiO} - \text{Cr}_2\text{O}_3$
system.

Integration path : $\frac{n_{\text{Cr}_2\text{O}_3}}{n_{\text{MnO}}} = \frac{0.752}{0.248}$ 

a_{NiO}	$-\log a_{\text{NiO}}$	$\frac{\partial n_{\text{NiO}}}{\partial n_{\text{Cr}_2\text{O}_3}}$	$-\log a_{\text{Cr}_2\text{O}_3}$	$a_{\text{Cr}_2\text{O}_3}$
0.200	0.6990	0.957	0	1.000
0.340	0.4685	0.992	0.2249	0.596
0.600	0.2218	1.012	0.4701	0.339
0.900	0.0458	1.083	0.6549	0.221
0.986	0.0061	1.114	0.6984	0.200

Integration path : $\frac{n_{\text{Cr}_2\text{O}_3}}{n_{\text{MnO}}} = \frac{0.655}{0.345}$

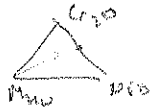
a_{NiO}	$-\log a_{\text{NiO}}$	$\frac{\partial n_{\text{NiO}}}{\partial n_{\text{Cr}_2\text{O}_3}}$	$-\log a_{\text{NiO}}$	$a_{\text{Cr}_2\text{O}_3}$
0.166	0.7800	0.859	0	1.000
0.200	0.6990	0.919	0.0726	0.846
0.340	0.4665	0.960	0.2890	0.514
0.600	0.2218	1.000	0.5254	0.298
0.900	0.0458	1.053	0.7084	0.196
0.972	0.0123	1.079	0.7440	0.180

TABLE XIII : (continued)

Integration path : $\frac{n_{\text{Cr}_2\text{O}_3}}{n_{\text{MnO}}} = \frac{0.522}{0.478}$

a_{NiO}	$-\log a_{\text{NiO}}$	$\frac{\partial n_{\text{NiO}}}{\partial n_{\text{Cr}_2\text{O}_3}}$	$-\log a_{\text{Cr}_2\text{O}_3}$	$a_{\text{Cr}_2\text{O}_3}$
0.030	1.5230	0.428	0	1.000
0.085	1.0720	0.517	0.2052	0.623
0.166	0.7800	0.715	0.4464	0.358
0.200	0.6990	0.751	0.5057	0.312
0.340	0.4685	0.835	0.6883	0.205
0.600	0.2218	0.898	0.9013	0.126
0.872	0.0595	0.930	0.0602	0.087

Integration path : $\frac{n_{\text{Cr}_2\text{O}_3}}{n_{\text{MnO}}} = \frac{0.50}{0.50}$



a_{NiO}	$-\log a_{\text{NiO}}$	$\frac{\partial n_{\text{NiO}}}{\partial n_{\text{Cr}_2\text{O}_3}}$	$-\log a_{\text{Cr}_2\text{O}_3}$	$a_{\text{Cr}_2\text{O}_3}$
0.030	1.5230	0.307	0.1549	0.700
0.085	1.0720	0.477	0.3326	0.465
0.166	0.7800	0.667	0.5560	0.278
0.200	0.6990	0.686	0.6108	0.245
0.340	0.4685	0.805	0.7820	0.165
0.600	0.2218	0.855	0.9868	0.103
0.840	0.0757	0.982	1.1138	0.077

TABLE XIII : (continued)

Integration path : $\frac{n_{\text{Cr}_2\text{O}_3}}{n_{\text{MnO}}} = \frac{0.483}{0.517}$

a_{NiO}	$-\log a_{\text{NiO}}$	$\frac{\partial n_{\text{NiO}}}{\partial n_{\text{Cr}_2\text{O}_3}}$	$-\log a_{\text{Cr}_2\text{O}_3}$	$a_{\text{Cr}_2\text{O}_3}$
0.030	1.5230	0.2469	0.3010	0.500
0.085	1.0720	0.4225	0.4498	0.355
0.166	0.7800	0.5974	0.6489	0.244
0.200	0.6990	0.6447	0.6804	0.209
0.340	0.4685	0.7575	0.8402	0.145
0.600	0.2218	0.8248	1.0360	0.092
0.805	0.0942	0.9760	1.1431	0.072

Integration path : $\frac{n_{\text{Cr}_2\text{O}_3}}{n_{\text{MnO}}} = \frac{0.468}{0.532}$

a_{NiO}	$-\log a_{\text{NiO}}$	$\frac{\partial n_{\text{NiO}}}{\partial n_{\text{Cr}_2\text{O}_3}}$	$-\log a_{\text{Cr}_2\text{O}_3}$	$a_{\text{Cr}_2\text{O}_3}$
0.030	1.5230	0.2240	0.3979	0.400
0.085	1.0720	0.3890	0.5323	0.294
0.166	0.7800	0.5720	0.7126	0.194
0.200	0.6990	0.6155	0.5888	0.174
0.340	0.4685	0.7300	0.9081	0.123
0.600	0.2218	0.8020	1.0980	0.0798
0.781	0.1073	0.9050	1.1911	0.0644

TABLE XIII : (continued)

$$\text{Integration path : } \frac{n_{\text{Cr}_2\text{O}_3}}{n_{\text{MnO}}} = \frac{0.452}{0.548}$$

a_{NiO}	$-\log a_{\text{NiO}}$	$\frac{\partial n_{\text{NiO}}}{\partial n_{\text{Cr}_2\text{O}_3}}$	$-\log a_{\text{Cr}_2\text{O}_3}$	$a_{\text{Cr}_2\text{O}_3}$
0.030	1.5230	0.1494	0.5229	0.300
0.085	1.0720	0.3280	0.6253	0.237
0.166	0.7800	0.5150	0.7899	0.162
0.200	0.6990	0.5950	0.8328	0.147
0.340	0.4685	0.6520	0.9719	0.107
0.600	0.2218	0.7480	1.1458	0.072
0.726	0.1390	0.7610	1.2080	0.062

$$\text{Integration path : } \frac{n_{\text{Cr}_2\text{O}_3}}{n_{\text{MnO}}} = \frac{0.565}{0.435}$$

a_{NiO}	$-\log a_{\text{NiO}}$	$\frac{\partial n_{\text{NiO}}}{\partial n_{\text{Cr}_2\text{O}_3}}$	$-\log a_{\text{Cr}_2\text{O}_3}$	$a_{\text{Cr}_2\text{O}_3}$
0.085	1.0720	0.5873	0	1.000
0.166	0.7800	0.7730	0.2646	0.544
0.200	0.6990	0.8180	0.3278	0.470
0.340	0.4685	0.8726	0.5217	0.301
0.600	0.2218	0.9305	0.7449	0.180
0.900	0.0458	0.9455	0.9096	0.123
0.925	0.0339	1.0080	0.9202	0.120

TABLE XIII : (continued)

Integration path : $\frac{n_{\text{Cr}_2\text{O}_3}}{n_{\text{MnO}}} = \frac{0.428}{0.572}$

a_{NiO}	$-\log a_{\text{NiO}}$	$\frac{\partial n_{\text{NiO}}}{\partial n_{\text{Cr}_2\text{O}_3}}$	$-\log a_{\text{Cr}_2\text{O}_3}$	$a_{\text{Cr}_2\text{O}_3}$
0.030	1.5230	0.105	0.6990	0.200
0.085	1.0720	0.316	0.7930	0.161
0.166	0.7800	0.453	0.9422	0.114
0.200	0.6990	0.546	0.9823	0.104
0.340	0.4685	0.572	1.1111	0.077

Integration path : $a_{\text{NiO}} = 0.03$

a_{MnO}	$-\log a_{\text{MnO}}$	$\frac{n_{\text{MnO}}}{n_{\text{Cr}_2\text{O}_3}}$	$-\log a_{\text{Cr}_2\text{O}_3}$	$a_{\text{Cr}_2\text{O}_3}$
0.0406	1.3915	0.920	0	1.000
0.0544	1.2644	0.980	0.1207	0.757
0.0633	1.1199	1.000	0.2635	0.545
0.0800	1.0969	1.072	0.2873	0.516
0.0980	1.0088	1.136	0.3847	0.412
0.1720	0.7645	1.181	0.6692	0.214
0.3440	0.4630	1.344	1.0322	0.093

TABLE XIII : (continued)

Integration path : $a_{\text{NiO}} = 0.085$

a_{MnO}	$-\log a_{\text{MnO}}$	$\frac{n_{\text{MnO}}}{n_{\text{Cr}_2\text{O}_3}}$	$-\log a_{\text{Cr}_2\text{O}_3}$	$a_{\text{Cr}_2\text{O}_3}$
0.0357	1.4473	0.800	0.000	1.000
0.0595	1.2255	0.918	0.191	0.643
0.0850	1.0710	0.981	0.338	0.459
0.0924	1.0343	0.998	0.375	0.422
0.1034	0.9855	1.071	0.425	0.376
0.1230	0.9101	1.132	0.508	0.310
0.2010	0.6968	1.218	0.759	0.174
0.3900	0.4089	1.320	1.125	0.075

TABLE XIV : Activity calculations of MnO in the MnO-NiO-Cr₂O₃ system.

Integration path : $\frac{n_{\text{MnO}}}{n_{\text{Cr}_2\text{O}_3}} = \frac{0.478}{0.522}$

a_{NiO}	$-\log a_{\text{NiO}}$	$-\frac{\partial n_{\text{NiO}}}{\partial n_{\text{MnO}}}$	$-\log a_{\text{MnO}}$	a_{MnO}
0.030	1.5230	0.346	1.391	0.040
0.085	1.0720	0.409	1.226	0.059
0.166	0.7800	0.520	1.091	0.081
0.200	0.6990	0.543	1.048	0.089
0.340	0.4685	0.594	0.918	0.121
0.600	0.2218	0.633	0.766	0.172
0.875	0.0580	0.642	0.699	0.200

Integration path : $\frac{n_{\text{MnO}}}{n_{\text{Cr}_2\text{O}_3}} = \frac{0.50}{0.50}$

a_{NiO}	$-\log a_{\text{NiO}}$	$-\frac{\partial n_{\text{NiO}}}{\partial n_{\text{MnO}}}$	$-\log a_{\text{MnO}}$	a_{MnO}
0.835	0.0783	0.6150	0.5896	0.270
0.600	0.2218	0.6016	0.6750	0.211
0.340	0.4685	0.5652	0.8180	0.152
0.200	0.6990	0.4956	0.9420	0.114
0.166	0.7800	0.4595	0.9810	0.104
0.085	1.0710	0.3528	1.0986	0.080
0.030	1.5230	0.2769	1.2630	0.055

TABLE XIV : (continued)

$$\text{Integration path : } \frac{n_{\text{MnO}}}{n_{\text{Cr}_2\text{O}_3}} = \frac{0.505}{0.495}$$

a_{NiO}	$-\log a_{\text{NiO}}$	$-\frac{\partial n_{\text{NiO}}}{\partial n_{\text{MnO}}}$	$-\log a_{\text{MnO}}$	a_{MnO}
0.0125	1.9030	0.285	1.363	0.0431
0.030	1.5280	0.289	1.264	0.0541
0.085	1.0720	0.382	1.112	0.0771
0.166	0.7800	0.479	0.987	0.1031
0.200	0.6990	0.502	0.946	0.1131
0.340	0.4685	0.561	0.821	0.1511
0.600	0.2218	0.603	0.676	0.2111
0.845	0.0731	0.616	0.585	0.2601

$$\text{Integration path : } \frac{n_{\text{MnO}}}{n_{\text{Cr}_2\text{O}_3}} = \frac{0.517}{0.483}$$

a_{NiO}	$-\log a_{\text{NiO}}$	$-\frac{\partial n_{\text{NiO}}}{\partial n_{\text{MnO}}}$	$-\log a_{\text{MnO}}$	a_{MnO}
0.030	1.5230	0.205	1.097	0.0801
0.085	1.0710	0.307	0.985	0.1031
0.166	0.7800	0.413	0.880	0.1321
0.200	0.6990	0.450	0.845	0.1431
0.340	0.4685	0.530	0.734	0.1851
0.600	0.2218	0.547	0.601	0.2511
0.807	0.0931	0.550	0.530	0.2951

TABLE XIV: (continue)

$$\text{Integration path: } \frac{n_{\text{MnO}}}{n_{\text{Cr}_2\text{O}_3}} = \frac{0.532}{0.468}$$

a_{NiO}	$-\log a_{\text{NiO}}$	$-\frac{\partial n_{\text{MnO}}}{\partial n_{\text{MnO}}}$	$-\log a_{\text{MnO}}$	a_{MnO}
0.030	1.5230	0.160	1.009	0.098
0.085	1.0710	0.272	0.912	0.123
0.166	0.7800	0.385	0.816	0.153
0.200	0.6990	0.423	0.783	0.165
0.340	0.4685	0.485	0.678	0.210
0.600	0.2218	0.490	0.558	0.277
0.781	0.1073	0.492	0.502	0.315

$$\text{Integration path: } \frac{n_{\text{MnO}}}{n_{\text{Cr}_2\text{O}_3}} = \frac{0.55}{0.45}$$

a_{NiO}	$-\log a_{\text{NiO}}$	$\frac{\partial n_{\text{NiO}}}{\partial n_{\text{MnO}}}$	$-\log a_{\text{MnO}}$	a_{MnO}
0.720	0.1426	0.4900	0.387	0.410
0.600	0.2218	0.4872	0.425	0.375
0.340	0.4685	0.4595	0.543	0.286
0.200	0.6990	0.3958	0.642	0.228
0.166	0.7800	0.3671	0.673	0.212
0.085	1.0710	0.2187	0.697	0.201
0.030	1.5230	0.1150	0.764	0.172

TABLE XIV: (continued)

$$\text{Integration path: } \frac{n_{\text{MnO}}}{n_{\text{Cr}_2\text{O}_3}} = \frac{0.572}{0.428}$$

a_{NiO}	$-\log a_{\text{NiO}}$	$-\frac{\partial n_{\text{NiO}}}{\partial n_{\text{MnO}}}$	$-\log a_{\text{MnO}}$	a_{MnO}
0.030	1.5230	0.074	0.463	0.344
0.085	1.0710	0.201	0.409	0.390
0.166	0.7800	0.304	0.330	0.468
0.200	0.6990	0.364	0.303	0.498
0.340	0.4685	0.381	0.217	0.607
0.455	0.3420	0.395	0.017	0.680

$$\text{Integration path: } a_{\text{NiO}} = 0.166$$

$a_{\text{Cr}_2\text{O}_3}$	$-\log a_{\text{Cr}_2\text{O}_3}$	$\frac{n_{\text{Cr}_2\text{O}_3}}{n_{\text{MnO}}}$	$-\log a_{\text{MnO}}$	a_{MnO}
0.358	0.4460	1.093	1.092	0.081
0.400	0.3980	1.118	1.144	0.072
0.500	0.3010	1.175	1.256	0.056
0.600	0.2218	1.271	1.352	0.044
0.700	0.1549	1.361	1.440	0.036
0.800	0.0969	1.463	1.522	0.030
0.900	0.0458	1.630	1.600	0.025
1.000	0	1.826	1.682	0.021

TABLE XIV: (continued)

Integration path: $a_{\text{NiO}} = 0.6$

$a_{\text{Cr}_2\text{O}_3}$	$-\log a_{\text{Cr}_2\text{O}_3}$	$\frac{n_{\text{Cr}_2\text{O}_3}}{n_{\text{MnO}}}$	$-\log a_{\text{MnO}}$	a_{MnO}
0.126	0.9000	1.0896	0.7670	0.171
0.200	0.6900	1.3230	1.0082	0.098
0.300	0.5229	2.0200	1.2864	0.052

Integration path: $a_{\text{Cr}_2\text{O}_3} = 1.0$ $N_{\text{Cr}_2\text{O}_3} = 0.50$

N_{NiO}	a_{NiO}	$-\log a_{\text{NiO}}$	$\frac{n_{\text{NiO}}}{n_{\text{MnO}}}$	$-\log a_{\text{MnO}}$	a_{MnO}
0.45	0.245	0.611	9.000	2.020	0.0096
0.40	0.231	0.636	4.000	1.870	0.0135
0.35	0.212	0.674	2.330	1.752	0.0177
0.30	0.191	0.719	1.500	1.671	0.0213
0.25	0.169	0.772	1.000	1.607	0.0247
0.20	0.145	0.839	0.660	1.552	0.0281
0.15	0.114	0.943	0.429	1.497	0.0319
0.10	0.080	1.097	0.250	1.447	0.0357
0.05	0.042	1.376	0.111	1.399	0.0399
0.01	0.035	1.456	0.087	1.392	0.0406

TABLE XIV: (continued)

Integration path: $a_{\text{NiO}} = 0.200$

$a_{\text{Cr}_2\text{O}_3}$	$-\log a_{\text{Cr}_2\text{O}_3}$	$\frac{n_{\text{Cr}_2\text{O}_3}}{n_{\text{MnO}}}$	$-\log a_{\text{MnO}}$	a_{MnO}
0.312	0.5057	1.091	1.0486	0.0894
0.400	0.3979	1.207	1.1710	0.0674
0.500	0.3010	1.289	1.2907	0.0512
0.600	0.2218	1.420	1.3980	0.0400
0.700	0.1549	1.543	1.4967	0.0319
0.800	0.0969	1.720	1.5910	0.0256
0.900	0.0458	2.460	1.6970	0.0201
1.000	0	2.940	1.8207	0.0151

Integration path: $a_{\text{NiO}} = 0.34$

$a_{\text{Cr}_2\text{O}_3}$	$-\log a_{\text{Cr}_2\text{O}_3}$	$\frac{n_{\text{Cr}_2\text{O}_3}}{n_{\text{MnO}}}$	$-\log a_{\text{MnO}}$	a_{MnO}
0.205	0.6883	1.065	0.917	0.1210
0.300	0.5229	1.279	1.110	0.0775
0.400	0.3979	1.454	1.282	0.0522
0.500	0.3010	1.714	1.434	0.0368
0.600	0.2218	2.882	1.583	0.0261